Science of the Total Environment 745 (2020) 140949

Contents lists available at ScienceDirect

Science of the Total Environment

journal homepage: www.elsevier.com/locate/scitotenv

Upwelling intensity modulates the fitness and physiological performance of coastal species: Implications for the aquaculture of the scallop *Argopecten purpuratus* in the Humboldt Current System

Laura Ramajo [a,b,*], María Valladares [c,d], Orlando Astudillo [a,d], Carolina Fernández [b,e], Alejandro B. Rodríguez-Navarro [f], Paul Watt-Arévalo [b], Manuel Núñez [e], Christian Grenier [f], Rocío Román [f], Paulina Aguayo [g,h], Marco A. Lardies [b,e], Bernardo R. Broitman [b,e], Pamela Tapia [i], Christian Tapia [i]

[a] Centro de Estudios Avanzados en Zonas Áridas (CEAZA), Coquimbo, Chile
[b] Center for the Study of Multiple-drivers on Marine Socio-Ecological Systems (MUSELS), Chile
[c] Centro de Innovación Acuícola AquaPacífico, Coquimbo, Chile
[d] Departamento de Biología Marina, Facultad de Ciencias del Mar, Universidad Católica del Norte, Coquimbo, Chile
[e] Departamento de Ciencias, Facultad de Artes Liberales, Universidad Adolfo Ibáñez, Santiago, Chile
[f] Departamento de Mineralogía y Petrología, Facultad de Ciencias, Universidad de Granada, Granada, Spain
[g] Department of Aquatic System, Faculty of Environmental Sciences & Environmental Sciences Center EULA Chile, Universidad de Concepción, Concepción, Chile
[h] Millennium Institute of Oceanography (IMO), Chile
[i] Ostimar S.A. Tongoy, Coquimbo, Chile

HIGHLIGHTS

- The activity of PLV upwelling centre affected the environmental variability of Tongoy Bay.
- Stronger upwelling generated more acidic and low oxygen environmental conditions.
- *A. purpuratus* showed biological mechanisms to handle acidified and hypoxic conditions.
- More intense upwelling events decreased the survivorship of *A. purpuratus*.
- A potential upwelling intensification will negatively impact the scallop aquaculture.

GRAPHICAL ABSTRACT

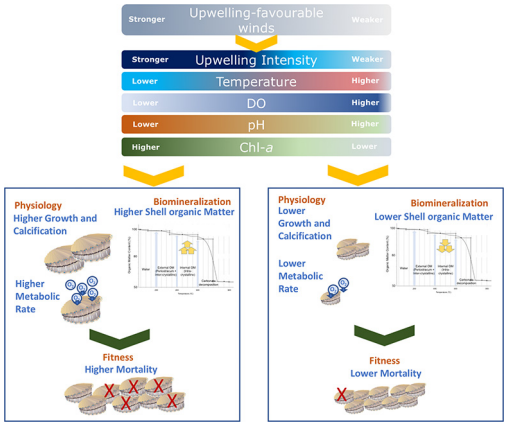

ARTICLE INFO

Article history:
Received 7 May 2020
Received in revised form 10 July 2020
Accepted 11 July 2020
Available online 19 July 2020

Editor: Henner Hollert

ABSTRACT

Understanding how marine species cope with the natural environmental variability of their native habitats will provide significant information about their sensitivity to the potential environmental changes driven by climate change. In particular, marine species inhabiting upwelling ecosystems are experiencing low seawater temperatures, as well as, acidic and low oxygen conditions as a consequence of the nature of the deep upwelled waters. Our study is focused on one of the most important socio-economical resources of the Humboldt Current System (HCS): the scallop *Argopecten purpuratus* which has been historically subjected to intensive aquaculture in areas influenced by upwelling processes. Here, a long-term field experiment was performed to understand how

* Corresponding author at: Centro de Estudios Avanzados en Zonas Áridas (CEAZA), Avenida Ossandón 877, Coquimbo, Chile.
E-mail address: laura.ramajo@ceaza.cl (L. Ramajo).

https://doi.org/10.1016/j.scitotenv.2020.140949

Keywords:
Scallops
Humboldt Current System
Ocean acidification
Ocean de-oxygenation
Aquaculture
Physiology

tolerant and well-locally-adapted is *A. purpuratus* to upwelling conditions by studying a set of fitness, physiological, and biomineralogical traits. Stronger upwelling generated a minor water column stratification, with lower temperatures, pH, and oxygen conditions. On the contrary, as upwelling weakened, temperature, pH, and oxygen availability increased. Finally, upwelling intensity also determined the number, duration, and intensity of the cooling and de-oxygenation events occurring in *A. purpuratus* habitat, as well as, the food availability (chlorophyll-*a* concentration, Chl-*a*). Physiologically, *A. purpuratus* was able to cope with stressful environmental conditions imposed by higher upwelling intensities by enhancing its metabolic and calcification rates, as well, producing higher concentrations of the shell organic matter. These physiological changes impacted the total energy budget, which was highly dependent on Chl-*a* concentration, and revealed important traits *trade-offs* with significant fitness costs (higher mortalities emerged when longer and more intense upwelling events succeed). Our study increases the knowledge about the physiological performance and tolerance of this important resource to the ocean acidification and ocean-deoxygenation imposed by variable upwelling intensities, as well as, its potential vulnerability under future changing conditions driven by a potential upwelling intensification.

1. Introduction

Coastal upwelling occurring at the Eastern Boundary Upwelling Systems (EBUS) is modulated by Ekman dynamics and large-scale thermocline processes (Barber and Smith, 1981; Pickett and Paduan, 2003; Messié et al., 2009). Equatorward winds force upwelling by transporting deeper colder and nutrient-rich waters to the surface where sunlight promotes the phytoplankton production (Sydeman et al., 2014). As a consequence, upwelling areas sustain the most productive ecosystems in the global ocean (Yáñez et al., 2017; FAO, 2018) with a major role in the marine primary production (7% of global marine production, Carr et al., 2002), and the worldwide fisheries (>20% global fish catches, Chavez and Messié, 2009) providing a high number of livelihoods and benefits to human society (Levin and Le Bris, 2015).

Global warming, as a consequence of increasing greenhouse gasses emissions from human activities, is responsible that more than 71% of coastal zones are experiencing a net heat gain (IPCC, 2019). However, this warming is not so evident in some EBUS as they have shown a decrease in their average thermal conditions for the last decades (Lima and Wethey, 2012; Falvey and Garreaud, 2009; IPCC, 2019). In particular, studies in the Humboldt Current System (HCS) have shown a consistent decrease of −0.36 °C and −0.07 °C per decade for the Peruvian and Chilean coasts, respectively (Gutiérrez et al., 2011; Seabra et al., 2015). Cooling trends in the HCS (Lima and Wethey, 2012; Falvey and Garreaud, 2009) have been attributed to changes in the magnitude (stronger) and duration (longer) of upwelling events as a consequence of a poleward shift in major atmospheric high-pressure Hadley cells that triggers an intensification the alongshore favourable-upwelling winds (Lu et al., 2007; Rykaczewski et al., 2015; Schneider et al., 2017; Aguirre et al., 2018; Jacob et al., 2018). However, temperature is only one of the multiple environmental variables subjected to change if upwelling intensifies, indeed an upwelling intensification might also redistribute the low-oxygen and high-CO_2 waters closer to shores. This will have widespread consequences on the coastal biogeochemical cycles and the physiology and fitness of all aerobic and calcifiying life, and, the multiple ecosystem services associated (García-Reyes et al., 2015; Levin, 2018; IPCC, 2019). Thus, to date, understanding how local biota residing upwelling-influenced habitats might be affected by a possible strengthening of the upwelling conditions is an urgent issue to be disentangled, especially because this information would help to predict future impacts, and take more adequate actions.

In Chile, fisheries are one of the most important socio-economic and productive activities with landings that exceeding 3.8 million tons per year (SERNAPESCA, 1978–2014). Furthermore, Chile stands out among the 10 major aquaculture countries with more than 2000 centres (Yáñez et al., 2017). In particular, the culture of aquatic species is one of the main 15th national economic activities with the highest growth during the last years (Chilean Central Bank, 2017) being an important source of employment in remote regions, and helping to reduce poverty (Ceballos et al., 2018; González-Poblete et al., 2020). In Chile, the native scallop *Argopecten purpuratus* is a bivalve species extensively subjected to aquaculture practices with production exceeding 4700 tons per year (SERNAPESCA, 2017). Its culture is mainly concentrated in northern Chile, specifically at Tongoy Bay (30°S), a northwest-facing embayment located upstream of Punta Lengua de Vaca (PLV), the most active upwelling centre along the Chilean coast (Rutllant & Montecino, 2002; Rahn and Garreaud, 2014). In this region, upwelling occurs year-round being more frequent during the austral spring-summer seasons (Moraga-Opazo et al., 2011; Bravo et al., 2016), and impacts on the environmental variability of the Tongoy Bay as a consequence of the sub-surface water properties (e.g. colder, more acidic, hypoxic, and richer-nutrient) (Torres et al., 1999; Torres and Ampuero, 2009; Ramajo et al., 2019).

To date, a large number of studies on *A. purpuratus* have focused on understanding how this species physiologically responds to changes in multiple drivers such as oxygen, temperature, or salinity (see Navarro and Gonzalez, 1998; Martinez et al., 2000; Soria et al., 2007). More recently, the impacts of the ocean acidification, ocean warming, and ocean de-oxygenation, as well as the role of the food availability have been assessed on multiple physiological and biomineralogical features (see Aguirre-Velarde et al., 2016; Lagos et al., 2016; Lardies et al., 2017; Ramajo et al., 2016a). However, to date, only one laboratory study has addressed, in the upwelling context, how combined changes in temperature, pH and oxygen affect the physiology and fitness of *A. purpuratus* (see Ramajo et al., 2019). Although many of these studies coincide about the great tolerance of *A. purpuratus* to multiple environmental conditions, to date, no studies have assessed how natural changes in the upwelling intensity might be affecting its physiological performance, and consequently their fitness. Accordingly, it is existing a high difficult to make accurate forecasts about how future conditions, potentially entailed by an upwelling intensification, could affect the entire socio-economic scenario linked to *A. purpuratus*.

Here, a long-term field experiment was performed to understand how *A. purpuratus* is impacted by the natural environmental dynamic of its habitat driven by upwelling processes of different intensity. To do that, key indicators of physiological performance and biological stress on multiple bivalve species such as metabolic, growth and calcification rates, as well as, shell bio-mineralogical properties (e.g. periostracum, shell organic matter) were monitored at different spatio-temporal scales with marked environmental differences modulated by differences in the intensity of favourable-upwelling winds.

2. Material and methods

2.1. Organisms collection

On 25th September 2017, 504 healthy juvenile scallops from wild populations (i.e. no shell damage and no shell parasites, see Basilio

et al., 1995) of similar size (~20 mm maximum length) growing at Tongoy Bay (30°16′S; 71°35′W) (Fig. 1) were provided by the scallop aquaculture company OSTIMAR S.A. Juvenile scallops were transported, under insulated conditions, to the laboratory situated at Tongoy (Liceo Carmen Rodríguez Henríquez), and further labeled with numbered bee tags glued onto the shells allowing their identification during the experiment (Fig. S1). At the laboratory, initial size (maximum large and maximum width) and initial buoyant weight were determined in all experimental juvenile scallops. During the initial measurements, juvenile scallops were maintained in aquaria at 14 °C, pH_{NBS} near to 8.0, and saturated oxygen conditions (>90%).

2.2. Experimental design

After the initial measurements, all experimental scallops were placed inside four scallop culture structures called by the industry *pearl nets*. Each *pearl net* contained two independent nets separated for approximately 25 cm (see Fig. S1). A total of 63 juvenile scallops with similar size [19.61 mm ± 0.11(SE), *one-way* ANOVA: $P = 0.265$] were randomly selected and placed at each net (see Fig. S1). *Pearl nets* were located in the culture line number 95 (hereafter, *L95*) of OSTIMAR S.A. company (30°15′26″S; 71°30′8″W) (Fig. 1) at two different experimental depths (two *pearl nets* at 9 m and two at 22 m depth). Here, the net of each *pearl net* was considered as an independent replicate (i.e. 4 replicates per depth treatment). Depth treatments were considered by two different reasons: (1) studies have shown how PLV upwelling impact over the water column stratification processes producing differential environmental conditions at different depths (see Moraga-Opazo et al., 2011), and (2) at Tongoy Bay, scallops are currently cultured along a great depth gradient (from 9 m to 30 m depth).

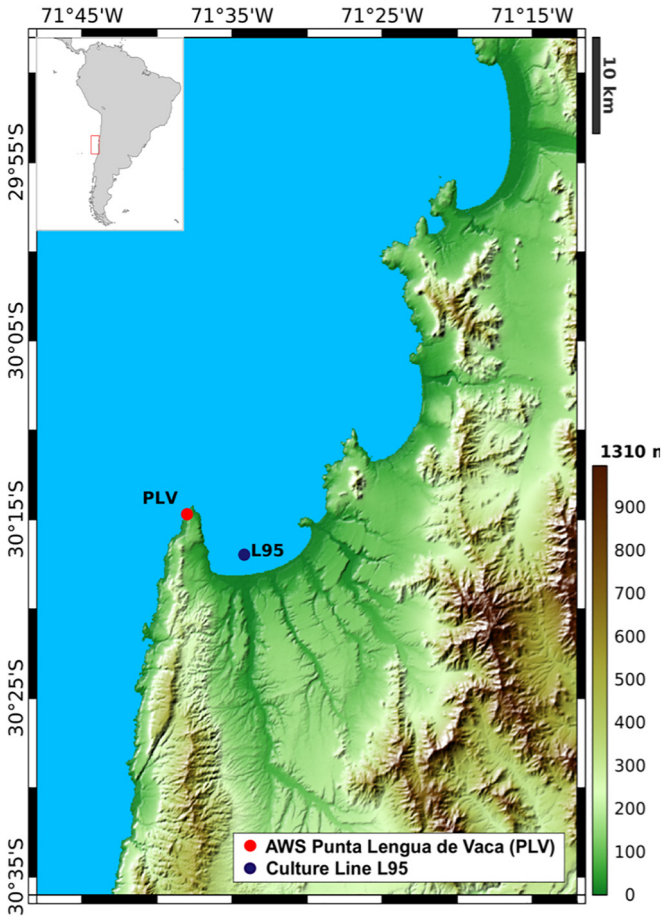

Fig. 1. Study site. Tongoy Bay coastal area with positions of the experiment (blue circle) deployed in the culture line *L95* and the location of the automatic weather station placed close to the upwelling centre Punta Lengua de Vaca (PLV) (red circle). (For interpretation of the references to color in this figure legend, the reader is referred to the web version of this article.)

The experiment lasted for a total of 183 days, and it was time-controlled three times (hereafter, *Period 1*, *Period 2*, and *Period 3*). The experimental *Period 1* lasted 50 days (28th September 2017 to 17th November 2017), *Period 2* lasted 50 days (21st November 2017 to 9th January 2018), and the *Period 3* lasted 83 days (12th January 2018 to 2nd April 2018). At the end of each experimental *Period*, the four *pearl nets* with the experimental scallops were removed from the *L95* and transported to the laboratory. Then, all alive scallops were transferred to aquaria with aerated seawater collected from each experimental depth (9 and 22 m). Further, multiple eco-physiological measurements (see below) were performed, and dead organisms were counted. After measurements, alive scallops were returned to the field in new and clean *pearl nets* following the same experimental design above described. Experimental scallops were assigned at the same experimental depth treatment where they came from, however, to avoid any experimental bias related to dense-dependency, some animals were relocated (inside same depth treatment) among nets to maintain the similar number of individuals per replicate.

2.3. Environmental conditions at Tongoy Bay

The intensity of wind-driven upwelling was determined using the continuous 10 m wind records from an Automatic Weather Station (AWS) at PLV (see Fig. 1). This well-exposed coastal location (~90 m from the coast) was taken as representative of the upwelling favourable conditions in the Tongoy Bay (Fig. 1) (Torres and Ampuero, 2009). Besides, multiple environmental variables were monitored (at high and low frequency) along the three experimental study *Periods*. Daily sea surface temperature (SST) was obtained from satellite-derived Multi-scale Ultra-high Resolution (MUR) analyses, and validated with in-situ SST measurements performed with a CTD probe (Ocean Seven 304Plus, Idronaut®) (see Fig. S2). At high frequency (each 15 min), dissolved oxygen (DO) (HOBO U26 Dissolved Oxygen Data Logger, ONSET®), and temperature (TidbiT Water Temperature Data Logger, ONSET®) were measured by attaching these sensors to the experimental *pearl nets* located at 9 and 22 m depth (see Fig. S1). At low frequency (weekly), pH_{NBS}, and total chlorophyll-*a* (Chl-*a*) conditions were determined by collecting water samples at each depth through a NISKIN bottle (5 L vol.). For pH_{NBS} measurements, 3 water samples per depth were analyzed within 60 min after water collection using a Metrohm 780 Meter (Metrohm®) connected to a combined electrode (Aquatrode Plus with Pt1000, Metrohm®) previously calibrated using three NBS buffers (Metrohm®) at 25 °C. For total Chl-*a* measurements, 2 water samples (200 mL volume) per depth (surface, 9 m and 22 m) were filtered through GF/F glass fiber filters (0.7 um) and frozen at −20 °C. At the laboratory, Chl-*a* was extracted in 90% acetone under dark conditions to further be measured. Total Chl-*a* was determined using a digital Turner fluorometer Designs (Trilogy Model) according to the standard procedures described by Strickland & Parsons (1968). Before measurements, fluorometer was calibrated using pure chlorophyll solutions (from 0.1 to 100 μgL^{-1}) in 90% acetone.

2.4. Physiological responses

For the three different experimental *Periods* and two depths, the metabolic (MR), growth (GR) and net calcification rates (NCR) of experimental scallops were determined. Gross GRs (hereafter, GGRs) were determined in all alive organisms as the difference of maximum length, maximum width and total area (estimated as an ellipsoid) between two consecutive experimental *Periods* and divided by the number of days elapsed between these *Periods* (mm day^{-1} or mm^2 day^{-1}). Further, GGRs were normalized by body size (hereafter, SGRs) to exclude the

ontogenic factor (i.e. differential amount of energy assigned to growth during the different life-stages, see Von Bertalanffy, 1964). To do that, individual GGRs were divided by the maximum shell length of each individual at the beginning of each *Period*. In the case of SGRs based on area measurements, GGRs were divided by the area of each individual at the beginning of each *Period*. NCRs, for all alive individuals, were estimated by using the buoyant weight technique (Davies, 1989). Buoyant weight was converted into shell dry weight using the seawater density (average conditions at Tongoy Bay, salinity = 34‰, temperature = 14 °C, see Ramajo et al., 2019), and the density of calcite (2.71 g cm^{-3}) (see Ramajo et al., 2016a). Finally, NCRs were computed as the change in the shell dry weight between two consecutive experimental *Periods*, and normalized by the initial shell dry weight of the individuals (mg $CaCO_3$ day^{-1} g^{-1}). MRs were determined by measuring the oxygen consumption of 5 individual scallops per replicate (net) (n = 20 per depth) at the end each *Period*. For MR measurements, experimental scallops were incubated individually by using respirometric chambers of variable volume (depending of the shell size of the scallop) at 14 °C (annual average temperature at the Tongoy Bay, see Ramajo et al., 2019). Temperature during the measurements was controlled by an automated temperature chiller (BOYU, Model L075). MRs were measured by using an optical fiber system (Mini Oxy-4 Respirometer, PreSens, Regensburg, Germany). Before measurements, experimental individuals fasted for 48 h in filtered seawater (5 μm). MRs were normalized by the dry weight of each individual (mg O_2 h^{-1} g^{-1}). Finally, buoyant weight was used to estimate changes in the allometry slopes by fitting with maximum length shell for the three different *Periods* and two depths.

2.5. Biomineralogical responses

Between 5 and 10 *A. purpuratus* individuals per replicate (nets) (n = 20–40 per depth treatment) at the end of each *Period* were randomly selected and sacrificed. Shells of these specimens were used to explore the composition and structure of the shells and periostracum. Before mineralogical analyses were performed, all shells were thoroughly cleaned by sonication in water 3 times during 2 min to remove adhered organic matter. The mineral composition and microstructure organization of the shell at the outer surface were analyzed by 2D X-ray diffraction. Intact pieces of shell (1 × 1 cm), cut from the outer growth border, was analyzed by using an X-ray single crystal diffractometer (Bruker D8 Smart Apex), equipped with a CCD area detector of molybdenum radiation and a 0.5 nm diameter collimator. To measure the samples by reflection mode, the diffractometer ω and 2θ angles were set at 10° and 20°, respectively (Checa et al., 2014). 2D X-ray diffraction patterns were analyzed by XRD2DScan software 7.0 (PANalytical, The Netherlands). The angular scattering in the orientation calcite crystals was determined from the Full Width Half Maximum (FWHM) of peaks displayed in the intensity profile along the Debye ring of the 104 calcite reflection (104 gamma scan). The amount and type of shell organic matter in *A. purpuratus* were determined by thermogravimetric analyses (TGA). The weight loss events detected at specific temperature ranges were assigned to water loss (20 °C–180 °C), inter-crystalline organic matter (180 °C–400 °C) and intra-crystalline organic matter (400 °C–600 °C) (Rodríguez-Navarro et al., 2006). The organic chemical composition of the periostracum was determined by analyzing the outer shell surface at the growth border by Attenuated Total Reflectance-Fourier Transformed Infrared Spectroscopy (ATR-FTIR) with Jasco Model 6200 spectrometer. A total of 32 scans per measurement with a resolution of 2 cm^{-1} in the mid infrared region (4000 to 400 cm^{-1}) were used to determine the organic chemical periostracum composition. The relative percentage of proteins, polysaccharides and lipids were estimated from the absorption peak areas associated with the characteristic molecular group of each component (e.g., O-H:water; C–H:lipids or fatty acids; amide:proteins; C–O:carbonates; S-O:sulfates; COC:sugars/polysaccharides; see Fig. S3). Additionally, *A. purpuratus* shell morphology and microstructure were analyzed by high resolution scanning electron microscopy (SEM) using a Zeiss Gemini (Germany). Shell samples (intact and fractures) were observed after applying a carbon coating (Hitachi UHS evaporator). All instrumentation used for the biomineralogical analyses was housed at the Department of Mineralogy and Petrology (Sciences Faculty) and the Scientific Instrumentation Center (CIC) of the University of Granada.

2.6. Mortality

Dead organisms were counted at the end of each *Period* for both experimental depths. Mortality rates were estimated as the percentage of dead organisms per day (% day^{-1}).

2.7. Data analysis

Environmental and biogeochemical seawater properties (i.e. pH_{NBS}, temperature, DO and total Chl-*a*), based on the mean state (±standard error, SE), and their variability (coefficient of variation, CV), were established for the three experimental *Periods* at 9 m and 22 m depth. Environmental and biogeochemical variables differences at 9 m and 22 m depth were evaluated using Student *paired t*-tests. Regarding the upwelling estimates, the 30-min mean wind components (i.e. zonal and meridional) were rotated into a coordinate system approximately aligned with the direction of the coast. From those wind records, alongshore wind stress ($\tau_{alongshore}$, units = N m^{-2}) was calculated by using the bulk formula:

$$\tau_{alongshore} = \rho_a \times C_d \times |v|v$$

where ρ_a is the constant air density (1.22 kg m^{-3}), and C_d is the neutral drag coefficient varying with *v* (see Large and Pond, 1981; Gill, 1982). Following, the alongshore wind stress was used to calculate the upwelling index (M, units = m^2 s^{-1} per meter of coast) based on the cross-shore volume transport. Note that, due to volume conservation, M is a direct measure of the vertical volume transport inherent with coastal upwelling (Bakun, 1975):

$$M = \frac{1}{\rho_w f}\tau_{alongshore}$$

where $\tau_{alongshore}$ is the alongshore wind stress, ρ_w is the density of seawater (assumed constant at 1024 kg m^{-3}), and f is the Coriolis parameter. Negative values of Ekman transport (M) indicate offshore transport (upwelling favourable winds), while positive values imply onshore transport (downwelling favourable winds) (Bakun, 1975). Given that upwelling, in the study region, is dominated by synoptic variability (see Renault et al., 2009), we removed the longer time scales of by subtracting a 30-day running mean from the daily average time series of Ekman transport (M), temperature and DO. This provides what is referred here as 'daily anomalies' which allow quantifying the different cooling and de-oxygenation events occurring at Tongoy Bay during the experiment.

Following Tapia et al. (2009), cooling and de-oxygenation events were identified when the temperature and DO anomalies steadily dropped from positive values, crossed the zero and returned to positive anomaly conditions (see Fig. 2). Further, by using this definition, it was possible to estimate the duration and the intensity of the cooling and de-oxygenation events for all *Periods* and both depths (Fig. 2). The intensity of cooling and de-oxygenation events was calculated as an integrated measure of the area between the negative segment of the anomaly curve and the zero-line, while the duration of the events was estimated by counting the number of days elapsed between the onset of a temperature or DO anomaly decrease and the subsequent zero-crossing when anomalies return to positive values. Additionally, the number of events was obtained by summing all events observed during

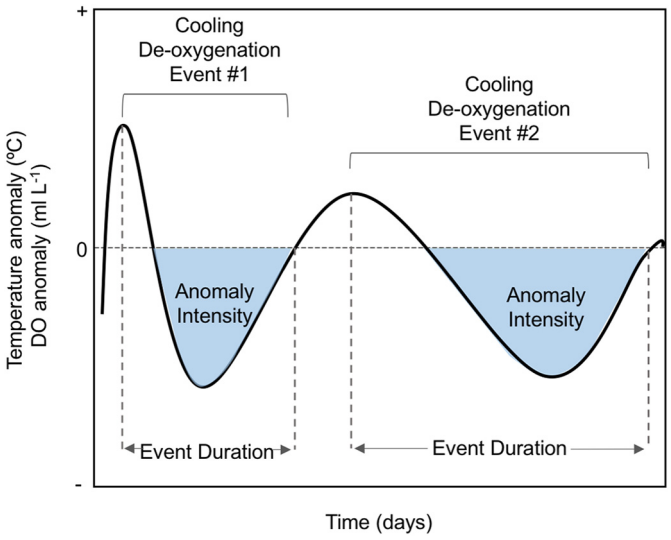

Fig. 2. Upwelling dynamics. Schematic of a daily anomaly time series covering two cooling (or deoxygenation) events with different intensity (duration and anomaly intensity) occurring at Tongoy Bay. The temporal extension of each anomalous event spans the onset of the drop-in temperature or DO until the variable anomaly returns to positive values. The intensity of the anomaly corresponds to the area (shaped in blue) between the negative curve and the *x*-axis. (For interpretation of the references to color in this figure legend, the reader is referred to the web version of this article.)
Based on Tapia et al. (2009) methodology.

each *Period* (see Fig. 2). Finally, the relationship between the Ekman transport (M) and the in-situ measurements of temperature and DO was quantified by using *Pearson* correlation analyses for all *Periods* and both depths.

Differences in GRs and NCRs were assessed by using hierarchical linear mixed-effects models. Four different model-types with different combinations of fixed effects were used to evaluate the independent, additive, and interactive effects of depth and experimental *Periods* (see Table S1). Random effects at the individual level were employed to control for potential organism effects, and random effects at the replicate (net) level were employed to control for potential 'replicate-effects' in all models. Linear mixed-effects models were estimated by using the *lme4* package of *R software, version* 3.5.0. Restricted maximum likelihood (REML) was used to fit each model, and to calculate unbiased estimates of parameter variance and standard error. The *AFEX*-package in *R* was used to obtain parameter *P*-values for the linear mixed-effects models, using the Kenward-Roger approximation for degrees-of-freedom. Optimal models were identified as those yielding the greatest number of significant ($P < 0.05$) fixed effects, with random effects assigned by AIC (see Table S2). Variance and standard deviation of the random effects (individual and replicate) are also reported.

The relationship between maximum shell length (SL) and shell weight (SW) for each *Period* and both depths was examined using standardized major axis analyses (SMA). Differences in slopes (b) within the same *Period* at both depths were estimated by using the scaling relationship $SL = aSW^b$. Allometry analyses were assessed by using the R-package *smatr* (R software, version 3.5.0.)

Differences on the MRs and mortality rates, as well as, some biomineralogical shell properties (e.g. shell crystal orientation, shell organic matter) were determined by using a *two-way* ANOVAs with depth and experimental *Periods* fixed as factors. When significant differences were found, Tukey HSD tests were performed to resolve differences between treatments (*Periods* and depths). Prior to ANOVA analyses, data were transformed (i.e. log) when was necessary to satisfy the assumptions of normality and homogeneity of variance. Normality and variance homogeneity were verified by using the Shapiro–Wilk and Levene tests. ANOVA analyses were performed by using R software (version 3.5.0.).

Finally, we used MANOVA analyses to determine differences in the relative chemical organic component forming periostracum during the experiment and between depths. In addition, Pearson's correlation analyses of the major bands in the FTIR spectrum from the periostracum (lipids, proteins, polysaccharides) and the shell mineral (CO_3) were performed to provide information about their relationships.

3. Results

3.1. Upwelling and environmental variability at Tongoy Bay

Coastal upwelling, induced by Ekman transport, at PLV exhibited a maximum intensity (large negative M values) during the first part of the study (spring 2017, *Period 1*) with a continuous reduction toward the end of the experiment (early-autumn 2018, *Periods 2* and *3*) (Fig. 3A; Table 2). Additionally, upwelling events (i.e. negative Ekman transport) were alternated with relaxation episodes (i.e. near zero Ekman transport values) on synoptic scales (from 1 to ~15 days, see Fig. 3A). At the surface, temperature (in average) showed a steady increase from *Period 1* to *Period 3* from 13.74 °C to 17.20 °C. However, at the middle of *Period 3* (February-2018), temperature started to decrease (see Fig. 3B), consistent with the onset of the autumn. On average, sea surface Chl-*a* showed an important reduction from *Period 1* to *Period 3*, however its variability showed an opposite pattern increasing from *Period 1* to *Period 3* (see Fig. 3E, Table 1).

Temperature, DO and pH_{NBS}, at both depths (9 m and 22 m) showed a similar pattern than SST, an increment from *Period 1* to *Period 3* (Table 1; Fig. 3B–D). On the contrary, total Chl-*a*, similar to observed at the surface, showed a consistent decrease from *Period 1* to *Period 3* at 9 m and 22 m depth (Fig. 3E). In average, *Period 1* showed the lowest temperature, DO and pH_{NBS} values comparing with *Period 2* and *Period 3*. On the other hand, *Period 3* showed the highest values in temperature (Fig. 3B), while pH_{NBS} and DO were maximum during the *Period 2* (Table 1; Fig. 3C–D). Significant differences in temperature, DO and pH_{NBS} between 9 m and 22 m depth were found for the three different *Periods* (see Table 1). In general, temperature, DO and pH_{NBS} were significantly higher at 9 m than at 22 m depth (Table 1; Fig. 3B–D). However, during the first part of the experiment (*Period 1*), these differences were smaller in comparison with the subsequent two experimental *Periods* (*Period 2* and *Period 3*) (Table 1; Fig. 3B–D). Although, Chl-*a* showed higher concentrations at 9 m than at 22 m depth, these differences were only significant during *Period 2* (Table 1; Fig. 3E).

In terms of variability (measured as CV), important differences were found among the three *Periods* (Tables 1 and 2). Ekman transport variability exhibited a clear increase from *Period 1* (CV ~ 50%) to *Period 3* (CV ~ 70%) (see Table 2). This agrees with the quasi-permanent upwelling conditions observed during the *Period 1* in relation to the upwelling-relaxation fluctuations that occurred during the *Periods 2* and *3* (Fig. 3A). DO variability was reducing from *Period 1* to *Period 3*, and it was always lower at 9 m than at 22 m depth (see Table 1). Chl-*a* variability (9 m and 22 m depth) was higher during the *Period 1* and *Period 2* (CV = 70–94%) in comparison with *Period 3* (see Table 1). Temperature (at surface, 9 m and 22 m depth) and pH_{NBS} (at 9 m and 22 m depth) showed low variability (CV < 8%), in comparison with the other environmental drivers, during the three *Periods*, and not clear differences were observed between 9 m and 22 m depth (Fig. 3B, D; Table 1).

From the analyses of temperature and DO anomalies, it was observed important changes in terms of the number, duration and intensity of the cooling and de-oxygenation events during the three *Periods* and both depths. The number of cooling and de-oxygenation events increased from *Period 1* to *Period 3*, while their intensity and temporal extension showed lower values during *Period 2* and *Period 3* in comparison with *Period 1* (see Table 2). Furthermore, wind-driven upwelling activity was significantly correlated with temperature and DO conditions during the majority of the *Periods* at 9 m and 22 m depth (see Table 2;

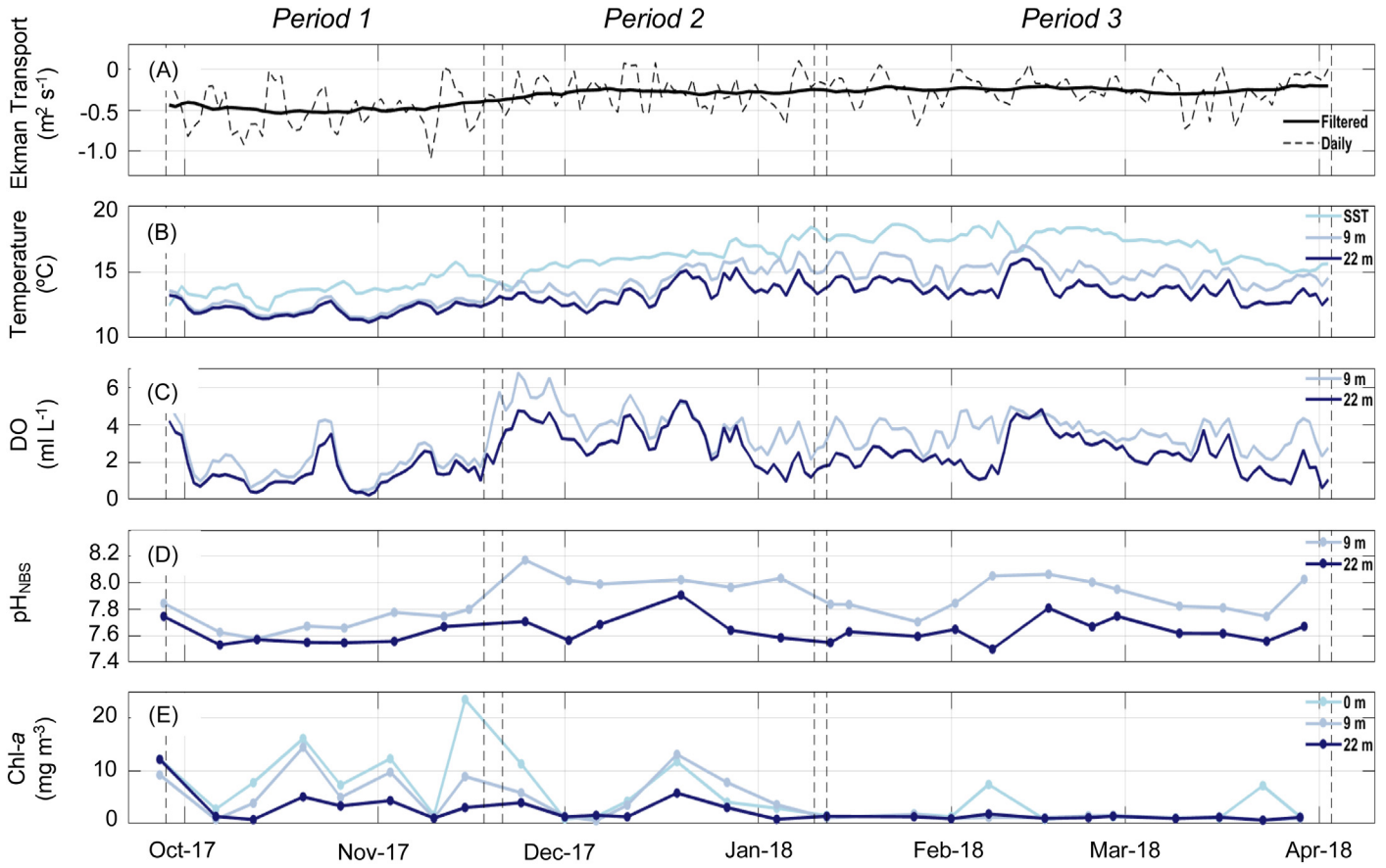

Fig. 3. Tongoy enviromental conditions. (A) Daily averaged and high-pass filtered time series of Ekman transport at PLV, in segmented and continuous lines, respectively. Daily averaged time series of (B) seawater temperature and (C) DO at 9 m (light blue) and 22 m (dark blue) depths. Weekly time series of (D) pH_{NBS} and (E) Chl-*a* concentration at 9 m (light blue) and 22 m (dark blue) depths. for the three experimental *Periods*. Vertical segmented lines separate the three experimental *Periods*. Sea surface temperature (SST) and Chl-a at surface are also showed. (For interpretation of the references to color in this figure legend, the reader is referred to the web version of this article.)

Table 1
Tongoy Bay environmental conditions. Temperature, dissolved oxygen (DO), pH_{NBS} and total chlorophyll-*a* (Chl-*a*) recorded during the three different experimental *Periods* and 9 m and 22 m depths at Tongoy Bay from September 2017 to April 2018. Sea surface temperature (SST) and Chl-*a* at surface are also showed. A summary of the paired comparison between depths (9 m and 22 m) within the same *Period* is also presented. Variability for each variable was estimated by the Coefficient of Variation (CV, %). Values are means ± SE. Bold texts show significant *P*-values at $\alpha = 0.05$. ND: Not determined. Sea surface temperatures were obtained from MUR SST analyses.

	Temperature (ºC)		Dissolved Oxygen (ml L^{-1})		pH_{NBS}		Total Chlorophyll-*a* (mg m^{-3})	
	Mean	CV (%)	Mean	CV (%)	Mean	CV (%)	Mean	CV (%)
Period 1 (Spring season)								
Surface	13.74±0.11	5.49	ND	-	ND	-	10.45±2.55	68.93
9m depth	12.34±0.08	4.36	1.96±0.16	56.19	7.71±0.01	1.21	6.63±1.68	71.62
22m depth	12.08±0.07	4.04	1.45±0.13	62.97	7.59±0.01	1.06	3.90±1.31	94.62
Paired *t*-test	-20.47		-12.28		-4.37		-1.93	
P-value	**0.000**		**0.000**		**0.005**		0.095	
Period 2 (Summer season)								
Surface	16.13±0.13	5.77	ND	-	ND	-	5.22±1.70	86.20
9m depth	14.43±0.15	7.10	4.17±0.16	26.32	8.03±0.01	0.90	5.59±1.49	75.30
22m depth	13.46±0.13	6.54	3.22±0.16	34.65	7.68±0.02	1.61	2.61±0.60	64.79
Paired *t*-test	-17.08		-11.05		-6.39		-2.96	
P-value	**0.000**		**0.000**		**0.001**		**0.021**	
Period 3 (Summer-autumn seasons)								
Surface	17.20±0.12	5.99	ND	-	ND	-	2.40±0.71	101.56
9m depth	15.04±0.09	5.65	3.54±0.08	20.34	7.89±0.01	1.56	1.20±0.09	25.71
22m depth	13.66±0.09	5.83	2.39±0.10	39.00	7.63±0.01	1.12	1.19±0.10	26.36
Paired *t*-test	-33.62		-14.12		-7.73		-0.11	
P-value	**0.000**		**0.000**		**0.000**		0.918	

Fig. 3). However, during the *Period 1* was registered the highest and significant correlation between Ekman transport and temperature-DO conditions ($R^2 > 0.78$). On the contrary, as time progressed during the experiment, the correlation values (though still significant) decreased (see Table 2).

3.2. Growth rates

GGRs (measured as changes in maximum large, maximum width and maximum area by time) increased from *Period 1* to *Period 3* at both depths (9 m and 22 m), being always lower in those scallops grown at 22 m than 9 m (Table S3; Fig. S5). Linear mixed models controlled for the random effects of individual and replicate confirmed that environmental conditions occurring at each experimental *Period* and at the different depths predicted significantly the GGRs observed ($P < 0.05$). On the other hand, no significant interaction between factors tested (*Periods* and depth) was detected for GGRs based in changes in the maximum shell length and maximum shell width (Fig. S5; Table S3). GGRs based in changes in the total shell area by time showed a significant interaction between the factors *Period* and depth (*P*-value < 0.0001) (Table S3; Fig. S5).

SGRs (measured as changes in maximum large, maximum width and maximum area by time and normalized by the initial size of the organisms) decreased from *Period 1* to *Period 3* at both depths (9 m and 22 m), being always SGRs higher in those scallops grown at 9 m than 22 m (Table 3; Fig. 4A–C). Linear mixed models showed similar results from the GGRs data analyses. The environmental conditions occurring at each experimental *Period* and at the different depths tested predicted significantly the SGRs observed (*P*-value < 0.05), where no significant interaction between factors tested (*Periods* and depth) was detected (Fig. 4A, B; Table 3) for any of the shell size variables measured (length, width and area).

3.3. Metabolic rates

MRs of experimental scallops were significantly different among the *Periods* (Table 4). Scallops during the *Period 2* showed significantly lower MRs in comparison with *Period 3*, but similar with *Period 1*. Scallop MRs during *Period 1* and *Period 3* were similar (Fig. 5A). No significant differences in the MRs were found to compare scallops grown at 9 m and 22 m depth in any of the *Periods* (Table 4; Fig. 5A).

Table 2
Upwelling index. Daily-averaged Ekman transport estimates (average conditions and variability) and its correlation (expressed by means of its coefficient of determination, R^2) with the temperature and DO conditions registered at Tongoy Bay during the experiment. The number, mean duration (days) and the average intensity of the cooling (ºC by day) and deoxygenation events (ml L^{-1} by day) registered by the three *Periods* at both experimental depths are shown. R^2 values were calculated by using the Ekman transport, temperature and DO filtered time series (see Methods section). Bold texts show significant *P*-values at $\alpha = 0.05$. Data shown are means ± SE.

Ekman Transport			R^2 (*P*-value)		Cooling Events			De-oxygenation Events		
Mean (m^2 s^{-1})	CV (%)	Depth	Temperature (ºC)	Dissolved Oxygen (ml L^{-1})	Number (#)	Duration (days)	Intensity (ºC by day)	Number (#)	Duration (days)	Intensity (ml L^{-1} by day)
Period 1 (Spring season)										
-0.50±0.04	50.55	9m	0.78 (**0.000**)	0.85 (**0.000**)	4	9.00±1.83	2.63±1.00	1	13.15	8.93
		22m	0.78 (**0.000**)	0.86 (**0.000**)	3	9.69±2.31	2.80±1.10	1	12.11	6.85
Period 2 (Summer season)										
-0.28±0.03	70.77	9m	0.09 (**0.039**)	0.07 (0.066)	5	5.16±1.40	1.57±0.64	5	5.94±1.48	2.77±0.93
		22m	0.10 (**0.026**)	0.12 (**0.015**)	5	6.13±1.47	1.80±0.77	4	7.90±1.42	3.77±1.35
Period 3 (Summer-autumn seasons)										
-0.25±0.02	71.27	9m	0.03 (0.119)	0.39 (**0.000**)	11	5.23±0.86	1.95±0.53	9	4.96±1.09	1.85±0.74
		22m	0.05 (**0.035**)	0.03 (0.118)	9	6.24±1.57	2.26±0.91	8	6.02±1.41	2.59±1.30

Table 3
Growth and calcification. Summary of statistical parameters for linear mixed effects models containing the most significant ($P < 0.05$) fixed effects (with random effects assigned by AIC) for size-normalized growth rates (length, width and area) and net calcification rates. Relative variance of the random effects (individual, replicate) are shown. Bold texts show significant *P*-values at $\alpha = 0.05$.

Fixed effects	Value	SE	*t*	*P*-value
Length (mm day^{-1} by size)				
Intercept	0.0087	0.0003	28.01	<**0.0001**
Depth	−0.0001	0.0000	−5.40	<**0.0001**
Period	−0.0011	0.0001	−10.44	<**0.0001**
Random effects	Variance	SD		
Individual	0.0000	0.0008		
Replicate	0.0000	0.0001		
Width (mm day^{-1} by size)				
Intercept	0.0098	0.0004	28.28	<**0.0001**
Depth	−0.0001	0.0000	−5.84	<**0.0001**
Period	−0.0013	0.0001	−10.80	<**0.0001**
Random effects	Variance	SD		
Individual	0.0000	0.0008		
Replicate	0.0000	0.0002		
Area (mm^2 day^{-1} by size)				
Intercept	0.0228	0.0009	26.44	<**0.0001**
Depth	−0.0002	0.0000	−5.57	<**0.0001**
Period	−0.0029	0.0002	−10.24	<**0.0001**
Random effects	Variance	SD		
Individual	0.0000	0.0024		
Replicate	0.0000	0.0004		
Net calcification rate (mg $CaCO_3$ day^{-1} g^{-1})				
Intercept	0.0035	0.0014	24.68	<**0.0001**
Period	−0.0050	0.0006	−7.78	<**0.0001**
Random effects	Variance	SD		
Individual	0.0000	0.0049		
Replicate	0.0000	0.0011		

3.4. Net calcification rates

Scallops exhibited positive NCRs during all *Periods* at both experimental depths (Fig. 5A). NCRs showed a decreasing trend throughout the time (from *Period 1* to *Period 3*) at 9 and 22 m depth (Table 3; Fig. 5B) being higher at 9 m than 22 m depth (Fig. 5B). Linear mixed models controlled for the random effects of individual and replicate confirmed that environmental conditions occurring at each *Period* and depth predicted significantly (*P*-value < 0.05) the NCRs of experimental scallops. No significant interaction between factors tested (*Periods* and depth) was detected (Table 4).

3.5. Allometry

Shell weight of *A. purpuratus* exhibited a significant scaling relationship with the shell maximum length (Fig. 6). The different slopes (b) of the scaling relationship $SW = aSL^b$, at different *Periods* and depths (*Period 1*: $b_{9m} = 2.82$ [2.64,2.99 CI]; $b_{22m} = 3.00$ [2.83,3.16 CI]; *Period 2*: $b_{9m} = 2.76$ [2.57,2.95 CI]; $b_{22m} = 3.00$ [2.85,3.25 CI]; *Period 3*: $b_{9m} = 2.66$ [2.44,2.87 CI]; $b_{22m} = 2.86$ [2.62,3.11 CI]) representing the increase in shell weight as the shell length increased (Fig. 6). Scaling relationship showed significant differences in slopes only during the *Period 2* (*P*-value = 0.028), but not during *Period 1* (*P*-value = 0.135) and *Period 3* (*P*-value = 0.200) when comparing between 9 m and 22 m depths (Fig. 6).

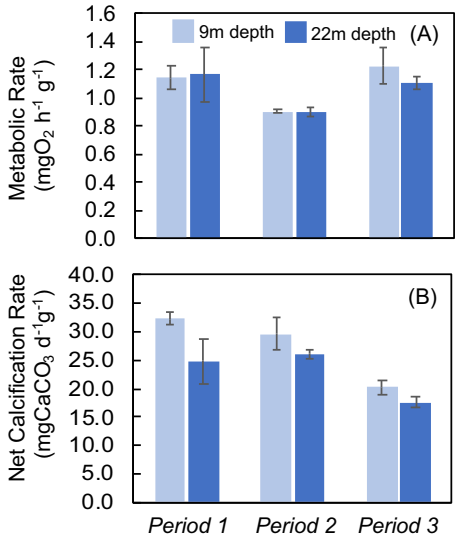

Fig. 5. Metabolism and calcification. (A) Metabolic rates (mg O_2 h^{-1} g^{-1}) and (B) net calcification rates (mm day^{-1}) of *A. purpuratus* scallops exposed to three different experimental *Periods* and two depths with dissimilar upwelling intensities and environmental conditions. Data are means ± SE.

Table 4
Metabolism and mortality. Effect of *Period* (three levels; *Period 1*: from September to November 2017; *Period 2*: November to January 2018; *Period 3*: from January to April 2018) and depth (two levels: 9 and 22m) on metabolic and mortality rates of *A. purpuratus*. Bold texts show significant *P*-values at $\alpha = 0.05$. Tukey HSD post hoc tests are shown.

Source	DF	MS	F	*P*-value	Post-hoc tests
Metabolic Rate (mgO_2 h^{-1} g^{-1})					
Period (P)	2	0.042	5.38	**0.015**	P1 = P3 > P2 = P1
Depth (D)	1	0.001	0.17	0.688	
P * D	2	0.002	0.30	0.746	
Residuals	18	0.008			
Mortality Rate (% day^{-1})					
Period (P)	1	0.000	8.15	**0.003**	P3 < P1 = P2 > P3
Depth (D)	1	0.000	6.57	**0.020**	9m < 22m
P * D	2	0.000	1.34	0.325	
Residuals	18	0.000			

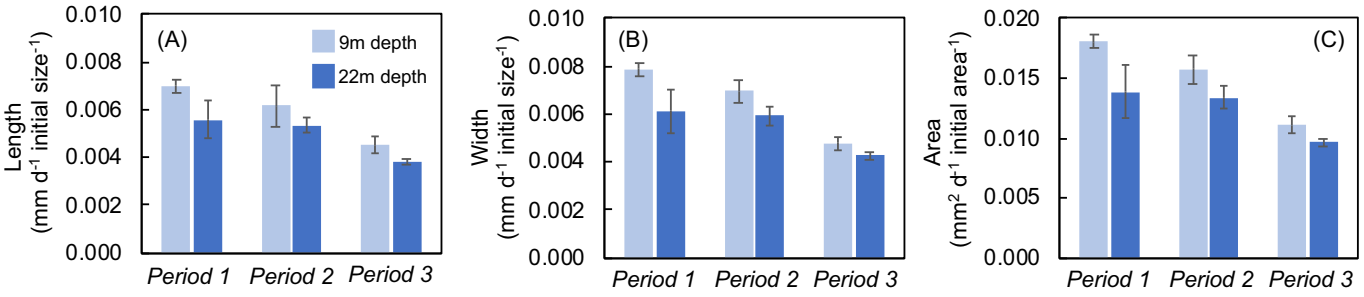

Fig. 4. Growth. Normalized growth rates (mm d^{-1} by body size) measured as changes in the maximum length (A), maximum width (B) and area (estimated as an ellipsoid) of *A. purpuratus* scallops exposed to three different experimental *Periods* and two depths with dissimilar upwelling intensities and environmental conditions. Data are means ± SE.

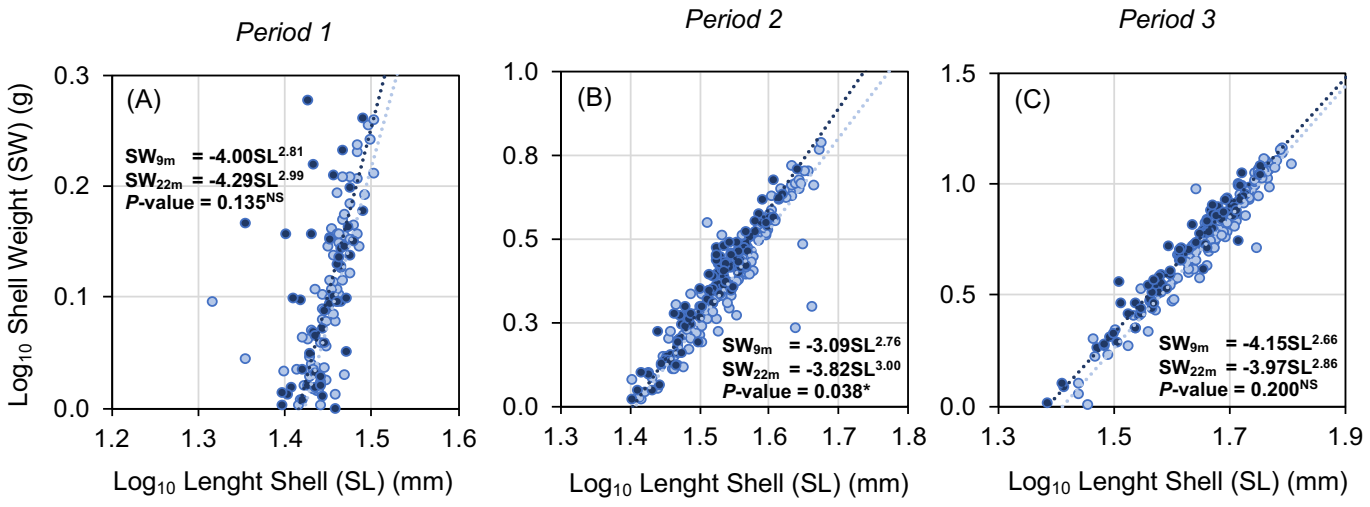

Fig. 6. Allometry. Scaling relationship between log_{10} maximum shell length (SL) and the log_{10} dry shell weight (SW) for *A. purpuratus* experimental scallops for the *Period 1* (A), *Period 2* (B) and *Period 3* (C) at both depths (9 and 22 m). The estimated parameters of the scaling relationship SL = *a*SW*b*, where *a* is the intercept and *b* is the slope of the fitter power regression for each *Period* and depth are shown. *P*-values of comparing slopes at each *Period* are also showed. NS = not significant; * = significant at α = 0.05.

3.6. Shell organic matter

TGA analyses were used to determine the total shell organic matter (inter- and intracrystalline) of *A. purpuratus* shells among the different experiment *Periods* and depths. Intercrystalline shell organic matter was significantly influenced by depth, being higher at 9 m than at 22 m depth. In addition, higher values of intercrystalline shell organic matter were recorded during *Period 2* in comparison with *Period 1* and *Period 3* which were similar between them (Fig. 8A; Table 5). On the other hand, the concentration of intracrystalline organic matter was higher during the *Period 1* in comparison with *Period 2* and *Period 3*, while depth did not affect the concentration of intracrystalline shell organic matter (Table 5; Fig. 8B).

3.7. Crystal shell orientation

DRX analyses showed that the intensity of Debye rings is concentrated in arcs, indicating that calcite crystals are preferentially oriented with their c-axis nearly perpendicular to the shell surface. Analyses of the angular scattering in the orientation of crystals and measured as the FWHM of the main peak in 104 gamma scans showed no significant differences neither between the different *Periods* (two-way ANOVA, *P*-value = 0.835) nor between depths (two-way ANOVA, *P*-value = 0.497) (Fig. 8C; Table 5).

Table 5
Shell organic matrix and crystal orientation. Effect of *Period* (three levels; *Period 1*: from September to November 2017; *Period 2*: November to January 2018; *Period 3*: from January to April 2018) and depth (two levels: 9 and 22m) on the shell organic matrix (intercrystalline and intra-crystalline) and shell crystal orientation (Full Width Half Maximum, FWHM), in scallops *A. purpuratus*. Comparison among *Periods* and depths were tested by using Tukey HSD *post hoc* tests. Bold numbers indicate significant *P*-values at α = 0.05.

Source	DF	MS	F	*P*-value	*Post-hoc tests*
Inter-crystalline Organic Matter (%)					
Period (P)	2	0.041	10.36	**0.000**	P2>P1=P3<P2
Depth (D)	1	0.018	4.49	**0.037**	9m>22m
P * D	2	0.001	0.21	0.812	
Residuals	82	0.004			
Intra-crystalline Organic Matter (%)					
Period (P)	2	0.167	23.41	**0.000**	P1>P2=P3
Depth (D)	1	0.021	2.91	0.092	
P * D	2	0.001	0.12	0.885	
Residuals	82	0.007			
FWHM (deg)					
Period (P)	1	95.44	0.45	0.503	
Depth (D)	1	97.94	0.47	0.497	
P * D	1	75.54	0.36	0.551	
Residuals	68	210.12			

3.8. Periostracum organic composition

ATR-FTIR analyses of the outer shell of experimental scallops revealed that the strongest IR bands correspond to carbonate (CO_3) signals. Still, conspicuous peaks from main periostracum organic components: proteins, lipids and polysaccharides were observed (Fig. S3). No significant differences in carbonate (CO_3), lipids, proteins and polysaccharides signals among specimens from different *Periods* (Wilks' Lambda = 0.88, *P*-value = 0.259), or between depths (Wilks' Lambda = 0.11, *P*-value = 0.080) (Fig. 7A, B) were observed. However, by analyzing the amount of organic components and CO_3 in all experimental organisms (independently of the *Period* and depth which were exposed), we observed a significant and negative correlation among the signal of CO_3 and the polysaccharides, proteins and lipids signals. In particular, polysaccharides were the organic compound that more contributed to the decrease in the CO_3 signal (R^2_{adj} = 0.90, *P*-value = 0.000), followed by proteins (R^2_{adj} = 0.28, *P*-value = 0.000) and lipids (R^2_{adj} = 0.11, *P*-value = 0.001) (Fig. 7C).

3.9. Shell morphology and microstructure

A. purpuratus shell morphology was characterized by conspicuous ribs that provided an undulating appearance of crests and valleys to the shell outer surface (Fig. S4). The shell surface showed a terraced morphology with edges parallel to the shell growth margin representing successive growth events. The shell surface was coated by a very thin periostracum that shows the topography of the underlaying mineral deposits (Fig. S4C, D). The periostracum showed a fibrous morphology with fibers running parallel to the shell edge. The periostracum fibers showed an inner nanogranular structure (granules are <100 nm in size), and the shell mineral was well-ordered and presented a layered structure made internally of laths of foliated calcite (Fig. S4E–G). The foliated calcite was made of long and slender beams of calcite crystals about 1 μm wide and 200 nm thick terminated with rhombohedral faces. The layer and lath surfaces were oriented parallel to the shell inner surface and the calcite beams were highly aligned and oriented perpendicular to the shell growth edge. Toward the

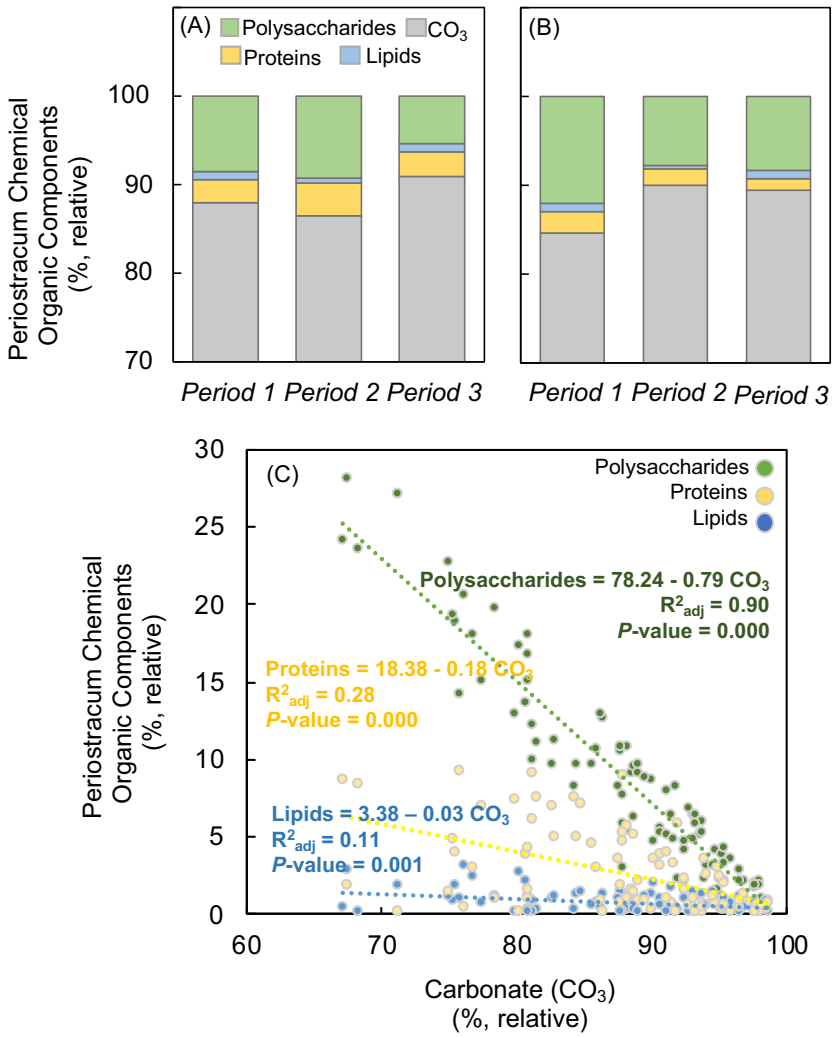

Fig. 7. Periostracum. Periostracum organic composition of *A. purpuratus* scallops exposed at (A) 9 m and (B) 22 m depth during three different experimental *Periods* with different upwelling intensity. (C) Relationship between the relative percentage of organic shell periostracum compounds (polysaccharides, proteins and lipids) and shell carbonate (CO_3).

outer shell surface and particularly in the ribs, the shell mineral loss its layered structure and becomes more disorganized being formed by massive aggregates of calcite microcrystals of uniform size (about 1 μm in size; Fig. S4H, I). No obvious and visible differences were noticed in shell morphology and/or microstructure characteristics among specimens collected at different *Periods* and depths.

3.10. Mortality

Experimental scallops showed significant differences in mortality during the different experimental *Periods* and between depths (Table 4). A visible negative trend in the mortality rates were detected from *Period 1* to *Period 3* (Fig. 9). Similar mortality rates were observed during *Period 1* and *Period 2* (*P*-value > 0.05), which were significantly higher in comparison with *Period 3* (Fig. 9). Mortality was always significantly lower at 9 m than 22 m depth (Fig. 9; Table 4).

4. Discussion

Predicting how marine biota will cope with future conditions requires an adequate understanding of the environmental dynamic, as well as, an improvement in the knowledge of how tolerant are marine species to heterogeneous environments. Here, focused on the Chilean scallop *A. purpuratus*, we addressed these two important points by recording, at high and low frequency, the environmental variability of the habitat where this species is cultured to further correlate it with changes in its fitness, physiological and biomineralogical performance. Our study showed how from austral spring 2017 to autumn 2018, Tongoy Bay was affected by favourable-upwelling winds with dissimilar intensities that modulated the temperatures, oxygen, pH, and productivity average conditions, as well as, their variability. Upwelling intensity also impacted the number, intensity, and duration of cooling and de-oxygenation events to which *A. purpuratus* organisms were exposed during the experiment. In response to this high environmental variability, *A. purpuratus* showed a significant phenotypic flexibility in multiple physiological (e.g. growth, metabolic, calcification rates), and biomineralogical responses (e.g. shell organic matter) that allowed it, in the majority of the cases, to adjust to punctual stressful conditions imposed by upwelling. However, under longer and more intense upwelling events, the survivorship was negatively impacted.

4.1. Effect of upwelling on Tongoy Bay environmental dynamic

Here, for the first time, it could be established how the coastal upwelling, based on Ekman transport, is capable of impact simultaneously the temperature, pH, dissolved oxygen, and Chlorophyll-*a* conditions at Tongoy Bay. Specifically, under higher Ekman transport (i.e. intense favourable-upwelling winds), Tongoy Bay showed reduced temperature,

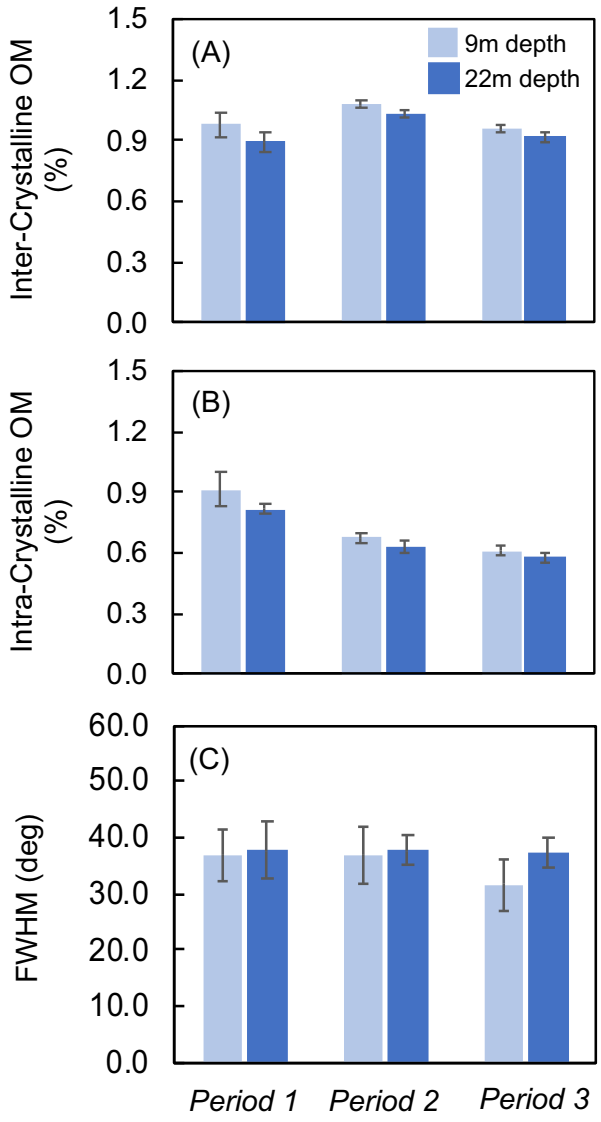

Fig. 8. Shell organic matter and crystal orientation. Intercrystalline (A), intracrystalline organic matter (B), and angular scattering in the orientation of calcite crystals (C) determined by TGA and 2D X-ray analyses at the outer shell surface of *A. purpuratus* shells that were exposed to three different experimental *Periods* and two depths with dissimilar upwelling intensities and environmental conditions. Data are means ± SE.

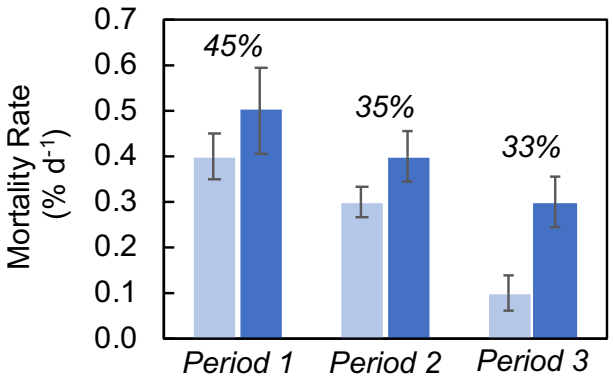

Fig. 9. Fitness. Mortality rates (% d^{-1}) of *A. purpuratus* scallops exposed to three different experimental *Periods* and two depths with dissimilar upwelling intensities and environmental conditions. Data are means ± SE. The total percentage of dead scallops with respect to the total by *Period* is shown above bars.

pH and DO conditions. On the contrary, weaker Ekman transport was associated with an increase in the aforementioned variables. Note that Ekman transport is one of the various processes that influence the spatial and temporal structure of upwelling. In particular, Ekman suction induced by cyclonic wind stress curl (Bravo et al., 2016; Astudillo et al., 2017), physical processes linked to coastal orography (Renault et al., 2015), SST wind coupling (Chelton et al., 2007), surface vertical mixing within the mixing layer and heat fluxes (Hong et al., 2013; Astudillo et al., 2019), could be impacting the upwelling circulation in the study region. Therefore, some limitations can exist to only consider the alongshore wind component, as Ekman transport does, to describe environmental conditions at Tongoy Bay. Nevertheless, the significant correlations found between Ekman transport and temperature and DO during the study would be indicating that Ekman transport is a good predictor of the environmental dynamic occurring at Tongoy Bay, especially under more intense favourable-upwelling wind conditions (higher correlations). Also, the magnitude and timing of Ekman transport were influential on the variability of DO, and Chl-*a* concentration, and, to a lesser extent, in pH and temperature.

Additionally, Ekman transport variability also had dissimilar impacts in environmental conditions at different depths of the water column. Csanady (1977) showed how the intensity and duration of the upwelling pulses (i.e. wind impulse) determines the water column stratification in upwelling-influenced coastal regions. During the experiment, Tongoy Bay showed a marked gradient in terms of temperature, pH and DO from the surface to deeper waters, however, this heterogeneity was lower under higher Ekman transport (*Period 1*). On the contrary, a weaker Ekman transport, in addition to the shallower summer mixed layer depth, favoured an increase in the water stratification. These results highlight the role of upwelling intensity on the vertical mixing processes occurring at Tongoy Bay (see Renault et al., 2012; Astudillo et al., 2019; Largier, 2020).

On average, Chl-*a* concentration followed an opposite pattern than temperature, pH, and DO during the experiment, showing higher values when Ekman transport was greater. This agrees with previous studies that have observed how chlorophyll biomass increases during the upwelling season as a consequence of an increase in the nutrients load at Tongoy Bay (Letelier et al., 2009). On the other hand, many other biological and physical processes could be responsible for the lowest Chl-*a* concentrations (~1.20 mg m^{-3}) recorded along the water column during the summer-autumn season. For instance, Lasker (1975) and Lasker & Zweifel (1978) noted that the alternation between upwelling activation and upwelling relaxation processes would be critical for the development of phytoplankton blooms. On the other hand, Cury and Roy (1989) and Bakun et al. (2015) determined the existence of an optimal range of upwelling that would be modulating the primary productivity dynamic, where the intensity of favourable-upwelling winds would be determining if nutrients can reach the euphotic layer to be used by the phytoplanktonic community. This was one of the probable causes of the decrease in the Chl-*a* concentrations as favourable-upwelling winds became weaker. However, the lack of nutrient data during the experiment, in addition to other factors (here also not addressed) such as changes in the phytoplankton community (e.g. Lee et al., 2013), phytoplankton size (e.g. Montecino and Quiroz, 2000; Shin et al., 2017), food-web dynamics (e.g. Armengol et al., 2019) could have affected the Chl-*a* concentrations observed during the experiment at Tongoy Bay. Also, biota consumption is an important factor that determines Chl-*a* dynamics (see Thompson et al., 2012). Specifically for Tongoy Bay, Uribe et al. (2001) determined that *A. purpuratus* culture supportsa high abundance and diversity of epibiont fauna (e.g. barnacles, bryozoans and ascidians). These species are significant filter feeders, and their abundance and feeding rates vary seasonally, being higher during the summer season when temperature increases (Uribe and Etchepare, 1998; Uribe et al., 2001; Soria et al., 2007). Although, this could also contribute to the significant

reduction in Chl-*a* concentrations during the summer season, here was not evaluated the epibiont presence and variability during the experiment.

Thought the analyses of the anomalies in temperature and DO, we were able to estimate how upwelling intensity impacted the number, duration and intensity of cooling and de-oxygenation events occurring among the different experimental *Periods* and depths. The results showed a high consistency with the previously discussed; i.e. the intensity and duration of the cooling and de-oxygenation events were proportional to the magnitude and temporal variability of the Ekman transport. Furthermore, the number of cooling and de-oxygenation events recorded showed an inverse association with their duration and intensity (i.e. a minor number of events, higher duration and intensity). This would be suggesting that during spring 2017, when stronger Ekman transport occurred, an overlapping of successive cooling and de-oxygenation events took place in the Tongoy Bay. On the contrary, as Ekman transport weakened, a major number of events with lower duration and lower intensity was observed suggesting that upwelling and non-upwelling conditions alternated (i.e. *Period 2* and *Period 3*). This pattern in the dynamic of the cooling and de-oxygenation events (number, duration and intensity) was consistent along the water column (e.g. higher number, intensity and duration of cooling and de-oxygenation events at 22 m than at 9 m depth) supporting the previously discussed about the role of the timing and intensity of favourable-upwelling winds in the vertical mixing processes of Tongoy Bay. Besides, and although DO dynamic in the water column showed a clear relationship with the intensity of favourable-upwelling winds, changes in the Chl-*a* concentration and the related oxygen consumption processes by phytoplankton could have also contributed to enhancing (or decrease) the intensity and duration de-oxygenation events during the experiment (e.g. Feng et al., 2014).

4.2. Effects of upwelling on A. purpuratus physiological performance

This major understanding of the upwelling impacts on Tongoy Bay environmental conditions lets to a better comprehension of the physiological performance of *A. purpuratus* in its habitat. Specifically, GRs (gross and normalized by body size) were significantly different among *Periods*, showing GGRs a steady increase along with the experiment at both depths. However, to normalize GGRs by body size (SGRs), an opposite tendency was observed which might be attributed to changes in the energetic costs of maintenance (and/or reproduction) that increase with size (and/or age) (Kooijman, 2000). Indeed, previous studies in *A. purpuratus* show that sexual maturity is achieved at sizes of 35 mm (Disalvo et al., 1984), which were reached during *Period 2* at both depths. The ontogenetic shift in the allocation of energy resources from somatic to reproductive production is widespread among iteroparous marine invertebrates (Bayne, 1993), such as scallop species (see Thompson and MacDonald, 1991). Indeed, allocation principle indicates that during early life stages (i.e. juveniles), somatic production and calcification reach a maximum, and then during maturation process growth and calcification become a decreasing function of age (Bricelj and Krause, 1992).

Differences found in the environmental conditions in terms of temperature, pH and DO along the water column during the experiment can explain the significant differences in both, GGRs and SGRs at 9 m and 22 m depths. Lower GGRs and SGRs were observed at deeper depths (22 m) for the three *Periods* where temperature, DO, and pH conditions were always lower than at shallower depths (9 m). This agrees with a recent laboratory experiment that observed how *A. purpuratus* juveniles exposed to a combined decrease in temperature, DO and pH grew significantly less (see Ramajo et al., 2019). However, food availability is a crucial factor to consider when stressful environmental conditions are present. A recent meta-analysis study (see Ramajo et al., 2016b) revealed that the negative impacts of OA on growth and calcification are reduced (or even null) if food is adequately supplied. This affirmation was based on the premise that food would be providing the energy necessary to maintain homeostasis by allowing the expression of multiple and energetic-costly biological mechanisms that cope with acidic conditions. Actually, Tongoy Bay showed important changes in the Chl-*a* concentration among the different *Periods* that might explain why higher SGRs were maintained when more intense upwelling conditions were present but higher Chl-*a* concentrations were observed. This also could explain the SGRs steady reduction in the following *Periods* with less stressful conditions but lower food availability, but also may have in part responsible for the lower SGRs observed at 22 m depth where Chl-*a* concentration was lower. Finally, the high MRs observed at the end of the *Period 1* supports the previously discussed in terms of food. Ramajo et al. (2016a), also in *A. purpuratus*, observed at the laboratory that higher GRs and MRs were supported by higher feeding rates, which also showed high correspondence with the amount of food supplied. Although we did not perform feeding rate measurements, the observed physiological responses; higher SGRs and increased MRs under high food availability might explain the better physiological performance of *A. purpuratus* under intensified upwelling conditions. Indeed, the reduced SGRs and MRs on those scallops growing at higher depth (22 m) where Chl-*a* was always lower, it would be supporting this hypothesis.

Complementary to food availability, the historical environmental variability to which species are exposed in their in native habitats determines the sensitivity, and the performance of marine species to climate stressors (Ramajo et al., 2016a, 2016c; Collier et al., 2019). Multiple biological mechanisms switch on under lower pH conditions in corals, bivalves, or foraminifers (see Hendriks et al., 2015), which has been attributed to evolutionary processes (i.e. acclimatization, see Collier et al., 2019). Indeed, Ramajo et al. (2019) determined that *A. purpuratus* population inhabiting at Tongoy Bay is highly adapted to the colder, acidic and hypoxic conditions imposed by upwelling, as this species has been constantly affected by these conditions. Specifically, metabolic up-regulation has been described as a response to stress as low pH on bivalve species such as mussels or scallops (Thomsen and Melzner, 2010; Lardies et al., 2014; Ramajo et al., 2016b, 2016c). This would be evidencing that *A. purpuratus* can express biological mechanisms to handle more intense upwelling conditions (i.e. *Period 1*). In addition, multiple studies have observed that temperatures also produce a significant increase in the MRs, which could explain the high MRs recorded during summer season (*Period 3*) (e.g. Aguirre-Velarde et al., 2016; Lagos et al., 2016; Ramajo et al., 2016b, 2019) when pH and oxygen conditions are more favourable.

4.3. Effects of upwelling on A. purpuratus shells

NCRs followed similar trends than SGRs, a sustained decrease from spring to autumn (from *Period 1* to *Period 3*). This suggests that as *A. purpuratus* individuals grew, the amount of the shell deposited calcium carbonate ($CaCO_3$) was lower, indicating a thinning of the shell. This is consistent with the observed in the scaling analysis where the slope of the relationship between the shell weight and shell length (i.e. increase in shell weight as the shell length increased) showed a consistent decrease from *Period 1* to *Period 3*. The lack of differences in slopes between 9 m and 22 m depth during the *Period 1* is coherent with the previously discussed (major homogenization of the water column), while for *Period 3* could be due to a mix of more favourable conditions at both depths or similar Chl-*a* concentrations.

NCRs did not show differences between depths within the same *Period*, which could indicate that calcification in *A. purpuratus* is more sensitive to greater changes in the environmental conditions (i.e. *Periods*) than those produced by depth. Several studies have determined that calcification is significantly impacted by changes in pH (e.g. Kroeker et al., 2013), temperature (e.g. Mancuso et al., 2019), salinity (Telesca et al., 2019), and oxygen conditions (e.g. Wijgerde et al., 2014). Specific studies performed on *A. purpuratus* have shown higher calcification

rates under lower pH conditions (Lagos et al., 2016; Ramajo et al., 2016b), or increasing temperatures (Aguirre-Velarde et al., 2016; Lagos et al., 2016; Ramajo et al., 2019). However, when pH and temperature were tested in combination with changes in the oxygen availability (i.e. hypoxia), not significant differences were found (see Ramajo et al., 2019). As it was discussed above, food availability (Chl-*a* concentration) could be responsible of modulating the *A. purpuratus* NCRs during our experiment. Indeed, calcification is an energetically-costly process (Palmer, 1983, 1992; Waldbusser et al., 2013) that consumes 75% and 410% more energy than somatic growth and reproduction, respectively (Paine, 1971). However, other processes, more than food availability, such as acclimatization could be responsible NCRs observed (discussed above).

NCRs represent the balance between shell gross calcification and shell dissolution (i.e. net accumulation of $CaCO_3$, organic matrix and inorganic carbon) in a specific moment (see Rodolfo-Metalpa et al., 2010). Hence, the study of biomineralization processes by examining shell properties such as the periostracum chemical composition, the amount of the shell organic matrix, or the shell crystal orientation provide relevant information about how the magnitude of changes observed in the NCRs. Periostracum is a thin organic layer covering the shell surface which is mainly composed of quinone-tanned sclerotized proteins and chitin polysaccharides (Beedham, 1958). Its function is to protect against shell dissolution (Tunnicliffe et al., 2009), but also acting as a substrate for $CaCO_3$ crystal nucleation (Checa et al., 2014; Harper et al., 2009). In addition, shell organic matrix also plays an important function to protect shell mineral dissolution, as inter- and intra-crystalline organic matter envelops the $CaCO_3$ crystals (Glover and Kidwell, 1993; Waldbusser et al., 2011). Previous studies have shown both structures, periostracum and shell organic matter, being seriously affected by environmental conditions (Green et al., 2004; Telesca et al., 2019; Grenier et al., 2020), which could, in turn, affect shell calcification as these components mediate shell biomineralization processes (Addadi and Weiner, 1992). In particular, a previous study on *A. purpuratus* detected important changes in the periostracum organic composition under different pH and food conditions (Ramajo et al., 2016a). Ramajo and colleagues found a higher relative amount of polysaccharides under lower pH conditions and lower food supply treatments, which was argued as a mechanism to increase the thickness of the periostracum and avoid shell dissolution under acidic conditions. In our study, the main organic compounds forming the *A. purpuratus* shell periostracum (e.g. polysaccharides, lipids and proteins) showed no consistent changes along with the experiment, but also did not differed at the different depths explored. Even though the periostracum in *A. purpuratus* is a thin layer (<100 nm), there was very large variability in the amount and composition of this protective organic coating with polysaccharides components having the greatest contribution to the total periostracum composition. This supports the idea that the amount of these organic components determine the thickness of this important organic layer (see Ramajo et al., 2016a).

On the other hand, unlike the periostracum, shell organic matter (inter- and intra-crystalline) did respond differently to changing environmental conditions during the different experimental *Periods*. Intra-crystalline organic matter showed higher values during intensified upwelling conditions, while intercrystalline organic matter was higher during the summer season (intermediate upwelling conditions). Additionally, intercrystalline shell organic matter was higher at 9 m than at 22 m depth. It should be noted that organic shell matrix component production is an energetically costly process (Harper et al., 2009) which could be reduced under more stressful conditions. Actually, observed changes in the periostracum or shell organic matter as a consequence of environmental changes could impact the nucleation of calcite crystals on the periostracum, and thus the $CaCO_3$ precipitation (Checa et al., 2014; Fitzer et al., 2012, 2014; Grenier et al., 2020). However, no changes in the crystal orientation of the *A. purpuratus* shells occurred during the different experimental *Periods* and depths analyzed. Moreover, all specimens showed a high degree of crystal orientation (low FWHM values) (Grenier et al., 2020) indicating that the functionality of shell organic matrix and their capacity to induce oriented nucleation of calcite crystals were not altered by environmental factors. Nevertheless, as previously discussed, shell calcification rates were significantly modified by the environment.

4.4. Fitness

A. purpuratus survivorship is highly linked to ecological processes such as competition by food (Basilio et al., 1995; Uribe and Etchepare, 1998; Uribe et al., 2001), or predation (López et al., 2000). In addition, *A. purpuratus* mortality is also size-dependent, being especially high at early-stages (Tarazona et al., 2007) which could explain the high mortality rates observed at the beginning of the experiment (*Period 1*), and the steady decrease as experimental scallops get bigger. Also, environmental changes such as changes in salinity (Uribe et al., 2003), temperatures (e.g. Ramajo et al., 2019), or even the strength of the currents, depth and turbidity can impact on *A. purpuratus* survivorship (see Brand, 2006). As it was discussed above, counteracting with stressful environmental conditions requires the expression of biological mechanisms, which are energetic costly and favour the apparition of physiological *trade-offs* (Stearns, 1989). *A. purpuratus* showed a high physiological performance (e.g. higher growth rates and metabolic rates, higher shell organic matter) when upwelling conditions were more intense demonstrating its high tolerance and resistance to stressful environmental conditions. However, also higher mortalities emerged when longer and more intense upwelling events succeed, that in combination with the size of the individuals (i.e. early stages are more susceptible to environmental changes), could explain the fitness changes of *A. purpuratus* during the experiment.

Indeed, the highest mortalities were observed during *Period 1* (45% of the total experimental scallops) when a higher physiological performance was detected evidencing the existence of an important *trade-off* between physiological performance and fitness. This would be determining that (1) although *A. purpuratus* is highly acclimated to upwelling conditions (see Ramajo et al. (2019)), this species is also very sensitive to longer and more intense upwelling conditions, (2) food availability is an important factor to maintain high physiological performance and avoid negative impacts on its fitness, and (3) a potential upwelling intensification certainly will have important and harmful consequences on the *A. purpuratus* aquaculture industry at Tongoy Bay.

Although our study might carry some limitations, many of them representative of field experiments (e.g. difficulty to attribute effects to a specific environmental driver), it complements the results previously obtained by laboratory experiments where multiple environmental drivers of upwelling, as well as, their future environmental projections were tested. Here, we visualize how *A. purpuratus* fitness and physiological-biomineralogical performance are impacted by changes in the upwelling intensity that occurs naturally in the habitat where this species is cultured. In addition, here we also provided evidence about which is the physiological tolerance of *A. purpuratus* to upwelling variability which helps to make better projections about how this important resource subjected aquaculture along the Chilean and Peruvian coasts could be affected by a scenario of upwelling intensification as GW increases. This information is highly relevant due to the key role that upwelling areas have in the global food security to endure the highest fisheries worldwide and suitable areas for aquaculture (FAO, 2018; Froehlich et al., 2018).

CRediT authorship contribution statement

Laura Ramajo: Conceptualization, Investigation, Formal analysis, Writing - original draft, Writing - review & editing. **María Valladares:** Investigation, Formal analysis, Writing - original draft, Writing - review & editing. **Orlando Astudillo:** Investigation, Formal analysis, Writing -

original draft, Writing - review & editing. **Carolina Fernández:** Investigation, Writing - review & editing. **Alejandro B. Rodríguez-Navarro:** Formal analysis, Resources, Formal analysis, Writing - original draft, Writing - review & editing. **Paul Watt-Arévalo:** Investigation, Writing - review & editing. **Manuel Núñez:** Investigation, Writing - review & editing. **Christian Grenier:** Formal analysis, Writing - review & editing. **Rocío Román:** Formal analysis, Writing - review & editing. **Paulina Aguayo:** Investigation, Writing - review & editing. **Marco A. Lardies:** Resources, Writing - review & editing. **Bernardo Broitman:** Resources, Writing - review & editing. **Pamela Tapia:** Resources, Writing - review & editing. **Christian Tapia:** Resources, Writing - review & editing.

Declaration of competing interest

The authors declare that the research was conducted in the absence of any commercial or financial relationships that could be construed as a potential conflict of interests.

Acknowledgements

We are very grateful to Julia Godoy, Jorge Guerra and all OSTIMAR S.A. staff for their valuable help and logistical support during all the experiment. We acknowledge to Nelson Lagos to provide CTD instrument. We thanks to Perla Araya and Oscar Leiva (Liceo Carmen Rodríguez Henríquez at Tongoy), and Miguel Martínez-Ledesma for all the help provided during the experiment. We acknowledge to Barbara Jacob for contributing to the result's discussion and Rocio Marquez-Crespo (CIC, UGR) for SEM analyses. We acknowledge the comments of Liz Harper and three anonymous rewiervers during the revision process.

Funding

This study was funded by FONDECYT Project #3170156 to LR and FONDECYT project #1140092 to MAL. LR, MAL, CF, PWA, and BB acknowledge the support from MINECON NC 120086 Project "Center for the Study of Multiple-drivers on Marine Socio-ecological Systems (MUSELS)" from the Ministerio de Economía, Fomento y Turismo. OA acknowledge the support from FONDECYT project #11190999. PA acknowledges the support of FONDECYT #3170732 and the Millennium Institute of Oceanography (IMO) (Grant #IC120019). BB, MV, PWA and MN acknowledge the support of the Proyecto Fortalecimiento Regional PRFVI0008 (CONICYT). CG, RR and ARN thank to the project CGL2015-64683-P (Ministerio de Ciencia e Innovación, Spain), and the 'Programa Operativo de Empleo Juvenil' (Garantía Juvenil) of European Union (EU).

Appendix A. Supplementary data

Supplementary data to this article can be found online at https://doi.org/10.1016/j.scitotenv.2020.140949.

References

Addadi, L., Weiner, S., 1992. Control and design principles in biological mineralization. Angew. Chem. 31, 153–169. https://doi.org/10.1002/anie.19920153.

Aguirre, C., García-Loyola, S., Testa, G., Silva, D., Farias, L., 2018. Insight into anthropogenic forcing on coastal upwelling off south-central Chile. Elem Sci Anth 6 (1), 59. https://doi.org/10.1525/elementa.314.

Aguirre-Velarde, A., Jean, F., Thouzeau, G., Flye-Sainte-Marie, J., 2016. Effects of progressive hypoxia on oxygen uptake in juveniles of the Peruvian scallop, Argopecten purpuratus (Lamarck, 1819). Aquaculture 451, 385–389. https://doi.org/10.1016/j.aquaculture.2015.07.030.

Armengol, L., Calbet, A., Franchy, G., Rodríguez-Santos, A., Hernández-León, S., 2019. Planktonic food web structure and trophic transfer efficiency along a productivity gradient in the tropical and subtropical Atlantic Ocean. Sci. Rep. 9, 2044. https://doi.org/10.1038/s41598-019-38507-9 (2019).

Astudillo, O., Dewitte, B., Mallet, M., Frappart, F., Rutllant, J.A., Ramos, M., et al., 2017. Surface winds off Peru-Chile: observing closer to the coast from radar altimetry. Remote Sens. Environ. 191, 179–196. https://doi.org/10.1016/j.rse.2017.01.010.

Astudillo, O., Dewitte, B., Mallet, M., Rutllant, J.A., Goubanova, K., Frappart, F., 2019. Sensitivity of the near-shore oceanic circulation off Central Chile to coastal wind profiles characteristics. Journal of Geophysical Research: Oceans 124, 4644–4676. https://doi.org/10.1029/2018JC014051.

Bakun, A., 1975. Daily and weekly upwelling indices, west coast of North America, 1967–73. NOAA Technical Report, NMFS SSRF-693. Department of Commerce, U.S. (114 pp).

Bakun, A., Black, B.A., Bograd, S.J., Garcia-Reyes, M., Rykaczewski, R.R., Sydeman, W.J., 2015. Anticipated effects of climate change on coastal upwelling ecosystems. Curr Clim Change Rep 1, 85–93. https://doi.org/10.1007/s40641-015-0008-4.

Barber, R., Smith, R., 1981. Coastal upwelling ecosystems. In: Longhurst, R. (Ed.), Analysis of Marine Ecosystems. Academic Press, pp. 31–68.

Basilio, C.D., Cañete, J.I., Rozbaczylo, N., 1995. Polydora sp. (Spionidae), un poliqueto perforador de las valvas del ostión Argopecten purpuratus (Bivalvia: Pectinidae) en Bahía Tongoy, Chile. Revista de Biología Marina 30, 71–77.

Bayne, B.L., 1993. Feeding Physiology of Bivalves: Time-Dependence and Compensation for Changes in Food Availability. In: Dame, R.F. (Ed.), Bivalve Filter Feeders. Nato ASI Series (Series G: Ecological Sciences). 33. Springer, Berlin, Heidelberg.

Beedham, G.E., 1958. Observations on the mantle of the lamellibranchia. J. Cell Sci. 3, 181e197.

Brand, Andrew R., 2006. Chapter 12 Scallop ecology: Distributions and behaviour. In: Shumway, Sandra E., Parsons, G. Jay (Eds.), Developments in Aquaculture and Fisheries Science. 35. Elsevier, pp. 651–744 ISSN 0167-9309. 9780444504821. https://doi.org/10.1016/S0167-9309(06)80039-6.

Bravo, L., Ramos, M., Astudillo, O., Dewitte, B., Goubanova, K., 2016. Seasonal variability of the Ekman transport and pumping in the upwelling system off central-northern Chile (~30° S) based on a high-resolution atmospheric regional model (WRF). Ocean Sci. 12, 1049–1065. https://doi.org/10.5194/os-12-1049-2016.

Bricelj, V.M., Krause, M.K., 1992. Resource allocation and population genetics of the bay scallop, Argopecten irradians irradians: effects of age and allozyme heterozygosity on reproductive output. Mar. Biol. 113, 253–261.

Carr, M.-E., Strub, P.T., Thomas, A.C., Blanco, J.L., 2002. Evolutions of the 1996–1999 La Niña and El Niño conditions off the western coast of south America: a remote sensing perspective. J. Geophys. Res. 108 (C12), 3236. https://doi.org/10.1029/2001JC001183.

Ceballos, A., Dresdner-Cid, J.D., Quiroga-Suazo, M.Á., 2018. Does the location of salmon farms contribute to the reduction of poverty in remote coastal areas? An impact assessment using a Chilean case study. Food Policy 75, 68–79.

Chavez, F.P., Messié, M., 2009. A comparison of eastern boundary upwelling ecosystems. Prog. Oceanogr. 83, 80–96. https://doi.org/10.1016/j.pocean.2009.07.032.

Checa, A.G., Pina, C.M., Osuna-Mascaro, A.J., Rodríguez-Navarro, A.B., Harper, E.M., 2014. Crystalline organization of the fibrous prismatic calcitic layer of the Mediterranean mussel *Mytilus galloprovincialis*. Eur. J. Mineral. 26, 495e505.

Chelton, D.B., Schlax, M.G., Samelson, R.M., de Szoeke, R.A., 2007. Global observations of large oceanic eddies. Geophys. Res. Lett. 34, L15606. https://doi.org/10.1029/2007GL030812.

Chilean Central Bank, 2017. CUENTAS NACIONALESDE CHILE. Evolución de la actividad económica en el año, 2017. https://www.bcentral.cl/areas/estadisticas/cuentas-nacionales-institucionales.

Collier, R.J., Baumgard, L.H., Zimbelman, R.B., Xiao, Y., 2019. Heat stress: physiology of acclimation and adaptation. Animal Frontiers 9 (1), 12–19. https://doi.org/10.1093/af/vfy031.

Csanady, G.T., 1977. Intermittent "full" upwelling in Lake Ontario. J. Geophys. Res. 82 (1977), 397–419.

Cury, P., Roy, C., 1989. Optimal environmental window and pelagic fish recruitment success in upwelling areas. Canadian Journal of Fishery and Aquatic Sciences 46, 670–680. https://doi.org/10.1139/f89-086.

Davies, P.S., 1989. Short-term growth measurements of corals using an accurate buoyant weighing technique. Mar. Biol. 101, 389–395. https://doi.org/10.1007/BF00428135.

Disalvo, L.H., Alarcon, E., Martínez, E., Uribe, E., 1984. Progress in mass culture of Chlamys (Argopecten) purpuratus Lamarck (1819) with notes on its natural history. Rev. Chil. Hist. Nat. 57, 35–45.

Falvey, M., Garreaud, R., 2009. Regional cooling in a warming world: recent temperature trends in the SE Pacific and along the west coast of subtropical South America (1979–2006). J. Geophys. Res. 114, D04102. https://doi.org/10.1029/2008JD010519.

FAO, 2018. The state of world fisheries and aquaculture 2018. Meeting the Sustainable Development Goals. Rome. Licence: CC BY-NC-SA 3.0 IGO.

Feng, Y., Fennel, K., Jackson, G.A., DiMarco, S.F., Hetland, R.D., 2014. A model study of the response of hypoxia to upwelling-favorable wind on the northern Gulf of Mexico shelf. J. Mar. Syst. 131, 63–73. https://doi.org/10.1016/j.jmarsys.2013.11.009.

Fitzer, S.C., Caldwell, G.S., Close, A.J., Clare, A.S., Upstill-Goddard, R.C., Bentley, M.G., 2012. Ocean acidification induces multi-generational decline in copepod naupliar production with possible conflict for reproductive resource allocation. J. Exp. Mar. Biol. Ecol. 418–419, 30–36. https://doi.org/10.1016/j.jembe.2012.03.00.

Fitzer, S.C., Phoenix, V.R., Cusack, M., Kamenos, N.A., 2014. Ocean acidification impacts mussel control on biomineralisation. Sci. Rep. 4, 6218. https://doi.org/10.1038/srep06218.

Froehlich, H.E., Gentry, R.R., Halpern, B.S., 2018. Global change in marine aquaculture production potential under climate change. Nat Ecol Evol 2, 1745–1750. https://doi.org/10.1038/s41559-018-0669-1.

García-Reyes, Marisol, Sydeman, William J., Schoeman, David S., Rykaczewski, Ryan R., Black, Bryan A., Smit, Albertus J., Bograd, Steven J., 2015. Under pressure: climate change, upwelling, and eastern boundary upwelling ecosystems. Front. Mar. Sci. 2, 109. https://doi.org/10.3389/fmars.2015.00109.

Gill, A., 1982. Atmosphere-Ocean Dynamics. Academic Press, New York, p. 662.

Glover, C.P., Kidwell, S.M., 1993. Influence of organic matrix on the post-mortem destruction of molluscan shells. The Journal of Geology 101, 729–747. https://doi.org/10.1086/648271.

González-Poblete, E., Kaczynski, Vladimir, Arias, Andrea Méndez, 2020. Marine coastal resources as an engine of development for the Lafkenche and Williche populations of southern Chile. Ocean Development & International Law 51 (1), 47–72. https://doi.org/10.1080/00908320.2019.1654248.

Green, M.A., Jones, M.E., Boudreau, C.L., Moore, R.L., Westman, B.A., 2004. Dissolution mortality of juvenile bivalves in coastal marine deposits. Limnol. Oceanogr. 49, 727–734.

Grenier, C., Román, R., Duarte, C., Navarro, J.M., Rodriguez-Navarro, A.B., Ramajo, L., 2020. The combined effects of salinity and pH on shell biomineralization of the edible mussel *Mytilus chilensis*. Environ. Pollut. 263, 114555. https://doi.org/10.1016/j.envpol.2020.114555.

Gutiérrez, J.L., Jones, C.G., Byers, J.E., Arkema, K.K., Berkenbusch, K., Commito, J.A., ... Wild, C., 2011. Physical ecosystem engineers and the functioning of estuaries and coasts. In: Wolanski, E., McLusky, D.S. (Eds.), Treatise on estuarine and coastal science, pp. 53–81.

Harper, E.M., Checa, A.G., Rodríguez-Navarro, A.B., 2009. Organization and mode of secretion of the granular prismatic microstructure of *Entodesma navicula* (Bivalvia: Mollusca). Acta Zool. 90, 132e141.

Hendriks, I.E., Duarte, C.M., Olsen, Y.O., Steckbauer, A., Ramajo, L., Moore, T., ... McCulloch, M., 2015. Biological mechanisms supporting adaptation to ocean acidification in coastal ecosystems. Estuaries. Coasts and Shelf Sciences 152, A1–A8.

Hong, X., Wang, S., Holt, T.R., Martin, P.J., O'Neill, L., 2013. Modulation of the sea surface temperature in the Southeast Pacific by the atmospheric low-level coastal jet. Journal of Geophysical Research: Oceans 118, 3979–3998. https://doi.org/10.1002/jgrc.20289.

IPCC, 2019. Summary for policymakers. In: Po€rtner, H.-O., Roberts, D.C., Masson-Delmotte, V., Zhai, P., Tignor, M., Poloczanska, E., Mintenbeck, K., Nicolai, M., Okem, A., Petzold, J., Rama, B., Weyer, N. (Eds.), IPCC Special Report on the Ocean and Cryosphere in a Changing Climate https://www.ipcc.ch/srocc/chapter/summary-for-policymakers/ (in press).

Jacob, B.G., Tapia, F.J., Quiñones, R.A., Montes, R., Sobarzo, M., Schneider, W., ... González, H.E., 2018. Major changes in diatom abundance, productivity, and net community T metabolism in a windier and dryer coastal climate in the southern Humboldt CurrenT. Progress in Oceanography 168 (2018), 196–209. https://doi.org/10.1016/j.pocean.2018.10.001.

Kooijman, S.A.L.M., 2000. Dynamic Energy and Mass Budgets in Biological Systems. Cambridge University Press, Great Britain (ISBN 0-521-78608-8).

Kroeker, K.J., Kordas, R.L., Crim, R., Hendriks, I.E., Ramajo, L., Singh, G.S., ... Gatusso, J.P., 2013. Impacts of ocean acidification on marine organisms: quantifying sensitivities and interaction with warming. Global Change Biology 19, 1884–1896. https://doi.org/10.1111/gcb.12179.

Lagos, N.A., Benitez, S., Duarte, C., Lardies, M.A., Broitman, B., Tapia, C., ... Vargas, C.A., 2016. Effects of temperature and ocean acidification on shell characteristics of *Argopecten purpuratus*: implications for scallop aquaculture in an upwelling-influenced area. Aquaculture Environment Interactions 8, 357–370. https://doi.org/10.3354/aei00183.

Lardies, M.A., Arias, M.B., Poupin, M.J., Manriquez, P.H., Torres, R., Vargas, C.A., ... Lagos, N.A., 2014. Differential response to ocean acidification in physiological traits of *Concholepas concholepas* populations. Journal of Sea Research 90, 27–134. https://doi.org/10.1016/j.seares.2014.03.010.

Lardies, M.A., Benitez, S., Osores, S., Vargas, C., Duarte, C., Lohrman, K., ... Lagos, N.A., 2017. Physiological and histopathological impacts of increased carbon dioxide and temperature on the scallops *Argopecten purpuratus* cultured under upwelling influences in northern Chile. Aquaculture 479, 455–466. https://doi.org/10.1016/j.aquaculture.2017.06.008.

Large, W.G., Pond, S.J., 1981. Open ocean momentum flux measurements in moderate to strong winds. J. Phys. Oceanogr. 11, 324–336. https://doi.org/10.1175/1520-0485(1981)011%3C0324:OOMFMI%3E2.0.CO;2.

Largier, J.L., 2020. Upwelling bays: how coastal upwelling controls circulation, habitat, and productivity in bays. Annu. Rev. Mar. Sci. 12 (1), 415–447. https://doi.org/10.1146/annurev-marine-010419-011020.

Lasker, S.E., 1975. SECTION OF BIOPHYSICS. Ann. N.Y. Acad. Sci. 37, 92–93. https://doi.org/10.1111/j.2164-0947.1975.tb03060.x.

Lasker, R., Zweifel, J.R., 1978. Growth and Survival of First-Feeding Northern Anchovy Larvae (Engraulis mordax) in Patches Containing Different Proportions of Large and Small Prey. In: Steele, J.H. (Ed.), Spatial Pattern in Plankton Communities. NATO Conference Series (IV Marine Sciences). vol 3. Springer, Boston, MA.

Lee, S.H., Yun, M.S., Kim, B.K., Joo, H.T., Kang, S.H., Kang, C.K., Whitledge, T.E., 2013. Contribution of small phytoplankton to total primary production in the Chukchi Sea. Cont Shelf Res 68, 43–50.

Letelier, J., Pizarro, O., Nuñez, S., 2009. Seasonal variability of coastal upwelling and the upwelling front off central Chile. J. Geophys. Res. 114, C12009. https://doi.org/10.1029/2008JC005171.

Levin, L.A., 2018. Manifestation, drivers, and emergence of open ocean deoxygenation. Annu. Rev. Mar. Sci. 10, 229–260. https://doi.org/10.1146/annurev-marine-121916-063359.

Levin, L.A., Le Bris, N., 2015. The deep ocean under climate change. Science 350, 766–768.

Lima, F.P., Wethey, D.S., 2012. Three decades of high-resolution coastal sea surface temperatures reveal more than warming. Nat. Commun. 3, 704. https://doi.org/10.1038/ncomms1713.

López, D., Riquelme, V., González, M., 2000. The effects of epibionts and predators on the growth and mortality rates of *Argopecten purpuratus* cultures in southern Chile. Aquacult. Int 8, 431–442. https://doi.org/10.1023/A:1009240202273.

Lu, J., Vecchi, G.A., Reichler, T., 2007. Expansion of the Hadley cell under global warming. Geophys. Res. Lett. 34, L06805. https://doi.org/10.1029/2006GL028443.

Mancuso, A., Stagioni, M., Prada, F., Scarponi, D., Piccinetti, C., Goffredo, S., 2019. Environmental influence on calcification of the bivalve *Chamelea gallina* along a latitudinal gradient in the Adriatic Sea. Sci. Rep. 9, 11198. https://doi.org/10.1038/s41598-019-47538-1.

Martinez, G., Brokordt, K., Aguilera, C., Soto, V., Guderley, H., 2000. Effect of diet and temperature upon muscle metabolic capacities and biochemical composition of gonad and muscle in Argopecten purpuratus Lamarck 1819. J. Exp. Mar. Biol. Ecol. 247, 29–34. https://doi.org/10.1016/S0022-0981(00)00143-X.

Messié, M., Ledesma, J., Kolber, D.D., Michisaki, R.P., Foley, D.G., Chavez, F.P., 2009. Potential new production estimates in four eastern boundary upwelling ecosystems. Progr. Oceanogr 83, 151–158. https://doi.org/10.1016/j.pocean.2009.07.018.

Montecino, V., Quiroz, D., 2000. Specific primary production and phyoplankton cell size structure in an upwelling area off the coast of Chile (30° S). Aquatic Science 62, 1–17. https://doi.org/10.1007/PL00001341.

Moraga-Opazo, J., Valle-Levinson, A., Ramos, M., Pizarro-Koch, M., 2011. Upwelling– triggered near–geostrophic recirculation in an equatorward facing embayment. Cont. Shelf Res. 31, 1991–1999. https://doi.org/10.1016/j.csr.2011.10.002.

Navarro, J., Gonzalez, C.M., 1998. Physiological responses of the Chilean scallop *Argopecten purpuratus* to decreasing salinities. Aquaculture 167, 315–327.

Paine, R.T., 1971. A short–term experimental investigation of resource partitioning in a New Zealand rocky intertidal habitat. Ecology 52, 1096–1106. https://doi.org/10.2307/1933819.

Palmer, A.R., 1983. Relative cost of producing skeletal organic matrix versus calcification: evidence from marine gastropods. Mar. Biol. 75, 287–292. https://doi.org/10.1007/BF00406014.

Palmer, A.R., 1992. Calcification in marine mollusks: how costly is it? Proc. Natl. Acad. Sci. U. S. A. 89, 1379–1382. https://doi.org/10.1073/pnas.89.4.1379.

Pickett, M.H., Paduan, J.D., 2003. Ekman transport and pumping in the California Current based on the U.S. Navy's high-resolution atmospheric model (COAMPS). J. Geophys. Res. 108, 3327. https://doi.org/10.1029/2003JC001902.

Rahn, D.A., Garreaud, R.D., 2014. A synoptic climatology of the near-surface wind along the west coast of South America. Int. J. Climatol. 34, 780–792. https://doi.org/10.1002/joc.3724.

Ramajo, L., Marba, N., Prado, L., Peron, S., Lardies, M.A., Rodríguez-Navarro, A.B., ... Duarte, C.M., 2016a. Biomineralization changes with food supply confer juvenile scallops (*Argopecten purpuratus*) resistance to ocean acidification. Global Change Biology 22, 2025–2037. https://doi.org/10.1111/gcb.13179.

Ramajo, L., Perez-León, E., Hendriks, I.E., Marba, N., Krause- Jensen, D., Sejr, M.M., ... Duarte, C.M., 2016b. Food supply confers calcifiers resistance to ocean acidification. Scientific Reports 6, 19374. https://doi.org/10.1038/srep19374.

Ramajo, L., Prado, L., Rodríguez-Navarro, A.B., Lardies, M.A., Duarte, C.M., Lagos, N.A., 2016c. Plasticity and trade-offs in physiological traits of intertidal mussels when confronting freshwater-induced environmental variation. Mar. Ecol. Prog. Ser. 553, 93–109.

Ramajo, L., Fernández, C., Núñez, Y., Caballero, P., Lardies, M.A., Poupin, M.J., 2019. Physiological responses of juvenile Chilean scallops (*Argopecten purpuratus*) to isolated and combined environmental drivers of coastal upwelling. ICES J. Mar. Sci. 76 (6), 1836–1849. https://doi.org/10.1093/icesjms/fsz080.

Renault, L., Dewitte, B., Falvey, M., Garreaud, R., Echevin, V., Bonjean, F., 2009. Impact of atmospheric coastal jet off central Chile on sea surface temperature from satellite observations (2000–2007). J. Geophys. Res. 114, C08006. https://doi.org/10.1029/2008JC005083.

Renault, L., Dewitte, B., Marchesiello, P., Illig, S., Echevin, V., Cambon, G., ... Ayers, J.K., 2012. Upwelling response to atmospheric coastal jets off central Chile: A modeling study of the October 2000 event. J. Geophys, Res. 117, C02030. https://doi.org/10.1029/2011JC007446.

Renault, L., Hall, A., McWilliams, J.C., 2015. Orographic shaping of U.S. West Coast wind profiles during the upwelling season. Climate Dyn. 46, 273–289. https://doi.org/10.1007/s00382-015-2583-4.

Rodolfo-Metalpa, R., Lombardi, C., Cocito, S., Hall-Spencer, J.M., Gambi, M.C., 2010. Effects of ocean acidification and high temperatures on the bryozoan *Myriapora truncata* at natural CO_2 vents. Mar. Ecol. 31, 447–456. https://doi.org/10.1111/j.1439-0485.2009.00354.x.

Rodríguez-Navarro, A.B., Cabral de Melo, C., Batista, N., Morimoto, N., Alvarez-Lloret, P., ... Arias, J.L., 2006. Microstructure and crystallographic-texture of giant barnacle (*Austromegabalanus psittacus*) shell. J. Struct. Biol 156 (2), 355e362. https://doi.org/10.1016/j.jsb.2006.04.009.

Rutllant, J., Montecino, V., 2002. Multiscale upwelling forcing cycles and biological response off north-central Chile. Rev. Chil. Hist. Nat. 75, 217–231.

Rykaczewski, R.R., Dunne, J.P., Sydeman, W.J., García-Reyes, M., Black, B.A., Bograd, S.J., 2015. Poleward displacement of coastal upwelling-favorable winds in the ocean's eastern boundary currents through the 21st century. Geophys. Res. Lett. 42, 6424–6431. https://doi.org/10.1002/2015GL064694.

Schneider, W., Donoso, D., Garcés-Vargas, J., Escribano, R., 2017. Water-column cooling and sea surface salinity increase in the upwelling region off central Chile driven by a pole-ward displacement of the South Pacific High. Prog. Oceanogr. 151, 38–48. https://doi.org/10.1016/j.pocean.2016.11.004.

Seabra, R., Wethey, D.S., Santos, A.M., Lima, F.P., 2015. Understanding complex biogeographic responses to climate change. Sci. Rep. 5, 12930. https://doi.org/10.1038/srep12930.

SERNAPESCA, 1978–2014. Anuarios Estadísticos de Pesca. Servicio Nacional de Pesca (SERNAPESCA). Ministerio de Economía, Fomento y Turismo, Chile.

SERNAPESCA (Servicio Nacional de Pesca y Acuicultura), 2017. Anuario 2017 - Subsector Acuicultura - Statistical Year book 2016 - Aquaculture. http://www.sernapesca.cl/sites/default/files/2017_desembarque_total_region_1.xls.

Shin, J.-W., Park, J., Choi, J.-G., Jo, Y.-H., Kang, J.J., Joo, H.T., ... Lee, S.H., 2017. Variability of phytoplankton size structure in response to changes in coastal upwelling intensity in the southwestern East Sea. Journal of Geophysical Research: Oceans 122, 10,262–10,274. https://doi.org/10.1002/2017JC013467.

Soria, R.G., Merino, G., Brand, E. von, 2007. Effect of increasing salinity on physiological response in juvenile scallops Argopecten purpuratus at two rearing temperatures. Aquaculture 270, 451–463. https://doi.org/10.1016/j.aquaculture.2007.05.018.

Stearns, S.C., 1989. The evolutionary significance of phenotypic plasticity: phenotypic sources of variation among organisms can be described by developmental switches and reaction norms. BioScience 39, 436–445. https://doi.org/10.2307/1311135.

Strickland, J.D.H., Parsons, T.R., 1968. A practical handbook of seawater analysis. J. Fish. Res. Board Can., Ottawa 311 pages.

Sydeman, W.J., García-Reyes, M., Schoeman, D.S., Rykaczewski, R.R., Thompson, S.A., Black, B.A., ... Bograd, S.J., 2014. Climate change and wind intensification in coastal upwelling ecosystems. Science 345, 77–80. https://doi.org/10.1126/science.1251635.

Tapia, F.J., Navarrete, S.A., Castillo, M., Menge, B.A., Castilla, J.C., Largier, ... Barth, J.A., 2009. Thermal indices of upwelling effects on inner-shelf habitats. Progress in Oceanography 83, 278–287. https://doi.org/10.1016/j.pocean.2009.07.035.

Tarazona, J., Espinoza, R., Solis, M., Arntz, W., 2007. Growth and somatic production of the fan scallop (Argopecten purpuratus) in Independencia Bay, Pisco (Peru) during El Niño and La Niña events. Rev. Biol. Mar. Oceanogr. 42, 275–285. https://doi.org/10.4067/S0718-19572007000300008 (online).

Telesca, L., Peck, L.S., Sanders, T., Thyrring, J., Sejr, M.K., Harper, E.M., 2019. Biomineralization plasticity and environmental heterogeneity predict geographical resilience patterns of foundation species to future change. Glob Change Biol. 2 (25), 4179–4193. https://doi.org/10.1111/gcb.14758.

Thompson, R.J., MacDonald, B.A., 1991. Physiological integrations and energy partitioning. In: Shumway, S.E. (Ed.), Scallops: Biology, Ecology and Aquaculture. Dev. in Aquaculture and Fisheries Science. vol. 21. Elsevier, New York, pp. 347–376.

Thompson, S.A., Sydeman, W.J, Santora, J.A, Black, B.A., Suryan, R.M., Calambokidis, J., ... Bograd, S.J., 2012. Linking predators to seasonality of upwelling: Using food web indicators and path analysis to infer trophic connections. Progress in Oceanography 101, 106–120. https://doi.org/10.1016/j.pocean.2012.02.001.

Thomsen, J., Melzner, F., 2010. Moderate seawater acidification does not elicit long–term metabolic depression in the blue mussel *Mytilus edulis*. Mar. Biol. 157, 2667–2676. https://doi.org/10.1007/s00227-010-1527-0.

Torres, R., Ampuero, P., 2009. Strong CO_2 outgassing from high nutrient low chlorophyll coastal waters off central Chile (30°S): the role of dissolved iron. Estuaries and Coast Shelf Sciences 83, 126–132. https://doi.org/10.1016/j.ecss.2009.02.030.

Torres, R., Turner, D., Silva, N., Rutllant, J., 1999. High short-term variability of CO2 fluxes during an upwelling event off the Chilean coast at 30°S. Deep-Sea Res. I 46, 1161–1179.

Tunnicliffe, V., Davies, K.T., Butterfield, D.A., Embley, R.W., Rose, J.M., Chadwick Jr., W., 2009. Survival of mussels in extremely acidic waters on a submarine volcano. Nat. Geosci. 2, 344e348.

Uribe, E., Etchepare, I., 1998. Investigación de variables que influyen en el desarrollo del piure blanco *Ciona intestinalis* (L) en el cultivo de ostión del norte Argopecten purpuratus. Informe al Fondo de Investigación Pesquera Chile. No. 9695 (220 pp).

Uribe, E., Lodeiros, C., Felix-Pico, E., Etchepare, I., 2001. Capítulo 13: Epibiontes de Pectínidos de Iberoamérica. In: Maeda-Martínez, A.N. (Ed.), Los Moluscos Pectínidos de Iberoamérica: Ciencia y Acuicultura. Editorial Limusa, México, pp. 249–266.

Uribe, E., Blanco, J.L., Yamashiro, C., 2003. Effect of salinity on the distribution of Argopecten purpuratus on the SW Pacific coast. Book of Abstracts, 14th International Pectinid Workshop, pp. 125–126 (St. Petersburg, FL, 2329 April 2003).

Von Bertalanffy, L., 1964. Basic concepts in quantitative biology of metabolism. Helgoländer Meeresun. 9, 5. https://doi.org/10.1007/BF01610024.

Waldbusser, G.G., Voigt, E.P., Bergschneider, H., Green, M.A., Newell, R.I.E., 2011. Biocalcification in the eastern oyster (*Crassostrea virginica*) in relation to long–term trends in Chesapeake Bay pH. Estuar. Coasts 34, 221–231. https://doi.org/10.1007/s12237-010-9307-0.

Waldbusser, G.G., Brunner, E.L., Haley, B.A., Hales, B., Langdon, C.J., Prahl, F.G., 2013. A developmental and energetic basis linking larval oyster shell formation to ocean acidification. Geophys. Res. Lett. 40, 2171–2176. https://doi.org/10.1002/grl.50449.

Wijgerde, T., Silva, C.I.F., Scherders, V., van Bleijswijk, J., Osinga, R., 2014. Coral calcification under daily oxygen saturation and pH dynamics reveals the important role of oxygen. Biology Open 3 (6), 489–493. https://doi.org/10.1242/bio.20147922.

Yáñez, E., Lagos, N.A., Norambuena, R., Silva, C., Letelier, J., Muck, K.-P., ... Stoffel, G., 2017. Impacts of climate change on marine fisheries and aquaculture in Chile. In: Phillips, B., Pérez-Ramírez, M. (Eds.), Climate Change Impacts on Fisheries and Aquaculture: A Global Analysis. Wiley-Blackwell, Hoboken, NJ, USA, pp. 239–332.